


ORIGINAL
ARTICLE

Distinct disruptions in Land's cycle remodeling of glycerophosphocholines in murine cortex mark symptomatic onset and progression in two Alzheimer's disease mouse models

Matthew W. Granger*[†], Hui Liu[‡], Caitlin F. Fowler*[†],
Alexandre P. Blanchard*[†], Matthew W. Taylor*[†], Samantha P. M. Sherman*[†],
Hongbin Xu*[†], Weidong Le[‡]§ and Steffany A. L. Bennett*[†] 

*Neural Regeneration Laboratory, Ottawa Institute of Systems Biology, Centre for Catalysis Research and Innovation, University of Ottawa Brain and Mind Research Institute, Ottawa, ON, Canada

[†]Department of Biochemistry, Microbiology, and Immunology, University of Ottawa, Ottawa, ON, Canada

[‡]Department of Neurology, Minhang Branch, Zhongshan Hospital, Fudan University, Shanghai, China

§Center for Clinical Research on Neurological Diseases, the 1st Affiliated Hospital, Dailan Medical University, Dailan, China

Abstract

Changes in glycerophosphocholine metabolism are observed in Alzheimer's disease; however, it is not known whether these metabolic disruptions are linked to cognitive decline. Here, using unbiased lipidomic approaches and direct biochemical assessments, we profiled Land's cycle lipid remodeling in the hippocampus, frontal cortex, and temporal-parietal-entorhinal cortices of human amyloid beta precursor protein (A β PP) over-expressing mice. We identified a cortex-specific hypo-metabolic signature at symptomatic onset and a cortex-specific hyper-metabolic signature of Land's cycle glycerophosphocholine remodeling over the course of progressive behavioral decline. When N5

TgCRND8 and A β PP^{Swe}/PSI^{dE9} mice first exhibited deficits in the Morris Water Maze, levels of *lyso*-phosphatidylcholines, LPC(18:0/0:0), LPC(16:0/0:0), LPC(24:6/0:0), LPC(25:6/0:0), the *lyso*-platelet-activating factor (PAF), LPC(O-18:0/0:0), and the PAF, PC(O-22:6/2:0), declined as a result of reduced calcium-dependent cytosolic phospholipase A $_2\alpha$ (cPLA $_2\alpha$) activity in all cortices but not hippocampus. Chronic intermittent hypoxia, an environmental risk factor that triggers earlier learning memory impairment in A β PP^{Swe}/PSI^{dE9} mice, elicited these same metabolic changes in younger animals. Thus, this lipidomic signature of phenoconversion appears age-independent. By contrast, in symptomatic N5 TgCRND8 mice, cPLA $_2\alpha$ activity

Received March 22, 2018; revised manuscript received July 4, 2018; accepted July 20, 2018.

Address correspondence and reprint requests to Dr Weidong Le, Center for Clinical Research on Neurological Diseases, the 1st Affiliated Hospital, Dailan Medical University, Dailan, 116021, China. E-mail: wdle@sibs.ac.cn and

Dr Hongbin Xu and Dr Steffany A. L. Bennett, India Taylor Lipidomic Research Platform, Neural Regeneration Laboratory, Department of Biochemistry, Microbiology, and Immunology, University of Ottawa, 451 Smyth Rd., Ottawa, ON K1H 8M5, Canada. E-mails: hxu@uottawa.ca; sbennet@uottawa.ca

Abbreviations used: AD, Alzheimer's disease; A β , amyloid-beta; A β PP, amyloid-beta precursor protein; COV, compensation voltage; cPLA $_2\alpha$, calcium-dependent cytosolic phospholipase A $_2\alpha$; DMS, differential mobility spectroscopy; EPI, enhanced product ion; FDR, false discovery rate; hA β PP, human amyloid-beta precursor protein; HPLC-ESI-MS/MS, high-performance liquid chromatography electrospray ionization tandem mass spectrometry; LPC(O), monoalkylglycerophosphocholine; LPC(P), monoalkenylglycerophosphocholine; LPCAT, lysophosphatidylcholine acyl-transferase; LPC, *Lyso*-phosphatidylcholine; PAF, platelet-activating factor acetylhydrolase; PAF, platelet-activating factor; PC(O), 1-alkyl,2-acylglycerophosphocholine; PC(P), 1-alkenyl,2-acylglycerophosphocholine; PC, diacylglycerophosphocholine; PIS, precursor ion scan; PLA $_2$, phospholipase A $_2$; PLS-DA, partial least squares-discriminant analysis; SRM, selected reaction monitoring; VIP, variable importance in projection; WT, wild type.

progressively increased; overall *Lyso*-phosphatidylcholines (LPC) and LPC(O) and PC(O-18:1/2:0) levels progressively rose. Enhanced cPLA₂α activity was only detected in transgenic mice; however, age-dependent increases in the PAF acetylhydrolase 1b α₁ to α₂ expression ratio, evident in both transgenic and non-transgenic mice, reduced PAF hydrolysis thereby contributing to PAF accumulation. Taken

together, these data identify distinct age-independent and age-dependent disruptions in Land's cycle metabolism linked to symptomatic onset and progressive behavioral decline in animals with pre-existing Aβ pathology.

Keywords: Alzheimer's disease, glycerophosphocholine, hypoxia, lipidomics, phospholipase A₂, platelet-activating factor. *J. Neurochem.* (2018) <https://doi.org/10.1111/jnc.14560>

[This article is related to the Special Issue "Vascular Dementia".](#)

Aberrant processing of the amyloid precursor protein (AβPP) to toxic amyloid-beta (Aβ) fragments and intraneuronal accumulation of neurofibrillary tangles composed of hyperphosphorylated tau are primary Alzheimer's disease (AD) pathologies (Bierer *et al.* 1995; Haass and Selkoe 2007). Their presence can be detected *in vivo* using amyloid positron emission tomography imaging or tracked by monitoring cerebrospinal fluid levels of Aβ₄₂, total tau, and phospho-tau (Bateman *et al.* 2012; Buchhave *et al.* 2012; Fagan *et al.* 2014). Longitudinal changes in these biomarkers indicate that AD neuropathology manifests decades before either autosomal-dominant or sporadic AD patients exhibit any signs of dementia (Bateman *et al.* 2012; Buchhave *et al.* 2012; Fagan *et al.* 2014; Dubois *et al.* 2016). This long latency, dubbed preclinical AD, suggests that additional metabolic dysfunctions are likely required to trigger symptomatic onset in patients with pre-existing AD pathology (Herrup 2010; Dubois *et al.* 2016). Identifying and targeting these critical metabolic changes (and their environmental causes) represents a novel, potentially transformative, means of reducing AD risk.

Previous lipidomic studies have reported that circulating glycerophosphocholine levels decline at symptomatic AD onset (Mapstone *et al.* 2014; Proitsi *et al.* 2017; Toledo *et al.* 2017). Metabolic determinants are unclear. Glycerophosphocholine metabolism is, in part, regulated by the Land's cycle. Enzymatic remodeling by the phospholipase A₂ (PLA₂) superfamily and lysophosphatidylcholine acyltransferases (LPCATs) coordinate the hydrolysis and re-acylation of both structural membrane glycerophosphocholines and bioactive second messengers (Supplemental Figure S1). At least 35 distinct PLA₂ isoforms are capable of cleaving the *sn*-2 fatty acyl chain from the glycerophosphocholine backbone (Burke and Dennis 2009). The specificity of these isoforms for different glycerophosphocholine substrates is not known beyond the preference of group IVa cPLA₂α for glycerophosphocholines with arachidonic acid at the *sn*-2 position (Kita *et al.* 2006). Cleavage generates free fatty acids and *lyso*-glycerophosphocholines defined by their *sn*-1 ester, ether (O), or vinyl ether (P)-linked hydrocarbon chains (Supplemental Figure S1). *Lyso*-phosphatidylcholines (LPC), *lyso*-platelet-activating factors (*lyso*-PAFs referred to

as LPC(O)), and alkenyl-*lyso*-PAFs (monoalkenylglycerophosphocholines, referred to as LPC(P)) metabolites can be subsequently remodeled by LPCATs (Supplemental Figure S1). Using acyl-CoA, LPCAT1-4 transfers a long-chain hydrocarbon to the *sn*-2 position of LPC, LPC(O), and LPC(P) regenerating diacylglycerophosphocholines (PC), 1-alkyl,2-acylglycerophosphocholines (PC(O)), and 1-alkenyl,2-acylglycerophosphocholines (PC(P)), respectively (Shindou and Shimizu 2009). Using acetyl-CoA, LPCAT 1 and 2 transfers an acetyl group to LPC(O) producing pro-inflammatory PC(O)-PAFs (Shindou and Shimizu 2009), PC(O)-PAFs can also be remodeled back to LPC(O) by three different PAF-acetylhydrolases (PAFAHs) (Prescott *et al.* 2000). Thus, each glycerophosphocholine is both a product and precursor in the Land's cycle.

Enzymatic dysregulation alters the glycerophosphocholine landscape over the course of AD. However, both increases (Farooqui and Horrocks 2006; Chalbot *et al.* 2009; Doody *et al.* 2015) and decreases (Ross *et al.* 1998; Gattaz *et al.* 2004; Smesny *et al.* 2008) in total PLA₂ activity are reported in CSF, platelets, and postmortem brain of AD patients (reviewed in (Bennett *et al.* 2013)). While LPC(O) levels are lower in patients diagnosed with 'probable' AD compared to cognitively normal controls (Mulder *et al.* 2003); LPC levels are higher in superior temporal and inferior parietal cortices of AD patients with severe end-state cognitive impairment and psychosis (Sweet *et al.* 2002). Total LPCAT activity is also elevated in postmortem human AD brain (Ross *et al.* 1998) with a shift in substrate preference of LPCAT2 from acyl- to acetyl-CoA upon exposure to Aβ₄₂ (Ryan *et al.* 2009). These changes effectively increase the remodeling of LPC(O) to PC(O)-PAF *in vitro* resulting in intraneuronal accumulation of PC(O)-PAFs that activates cyclin-dependent kinase 5 resulting in the hyperphosphorylation of tau on AD-associated epitopes (Ryan *et al.* 2009). Taken together, these data implicate changes in glycerophosphocholine metabolism in AD etiology. It is not, however, clear whether distinct metabolic disruptions mark different stages of AD cognitive decline.

To address this question, we used unbiased lipidomic approaches and direct biochemical assessments of both protein expression and enzymatic activity to profile glycerophosphocholine metabolism in the hippocampus, frontal

cortex, and temporal-parietal-entorhinal cortex in two human A β PP-over-expressing mouse models over the course of their behavioral decline. We show that group IVa cPLA₂ α activity decreases, reducing levels of specific LPC and LPC(O) in cortices when A β PP^{Swe}/PSI^{dE9} and N5 TgCRND8 mice first exhibit learning and memory impairments. Moreover, we show that chronic intermittent hypoxia, an environmental risk factor that accelerates the appearance of learning and memory deficits in A β PP^{Swe}/PSI^{dE9} mice (Liu *et al.* 2016), triggers these same changes in younger mice. We next asked whether these deficits were maintained in fully impaired animals. Surprisingly, we found that metabolic differences are reversed over the course of symptomatic progression. Group IVa cPLA₂ activity is elevated; LPC and LPC(O) levels rise; and remodeling of LPC(O) to PC(O)-PAF increases in the cortex of impaired N5 TgCRND8 mice. These changes are accompanied by an age-dependent shift in the expression of PAFAH1b α_1 and α_2 catalytic subunits that further reduces the hydrolysis of PC(O)-PAF over the course of normal aging resulting in accumulation of PC(O-18:1/2:0). Taken together, these data identify two defining disruptions in Land's cycle glycerophosphocholine metabolism in murine cortices linked to symptomatic onset and progressive behavioral decline in human A β PP mice.

Materials and methods

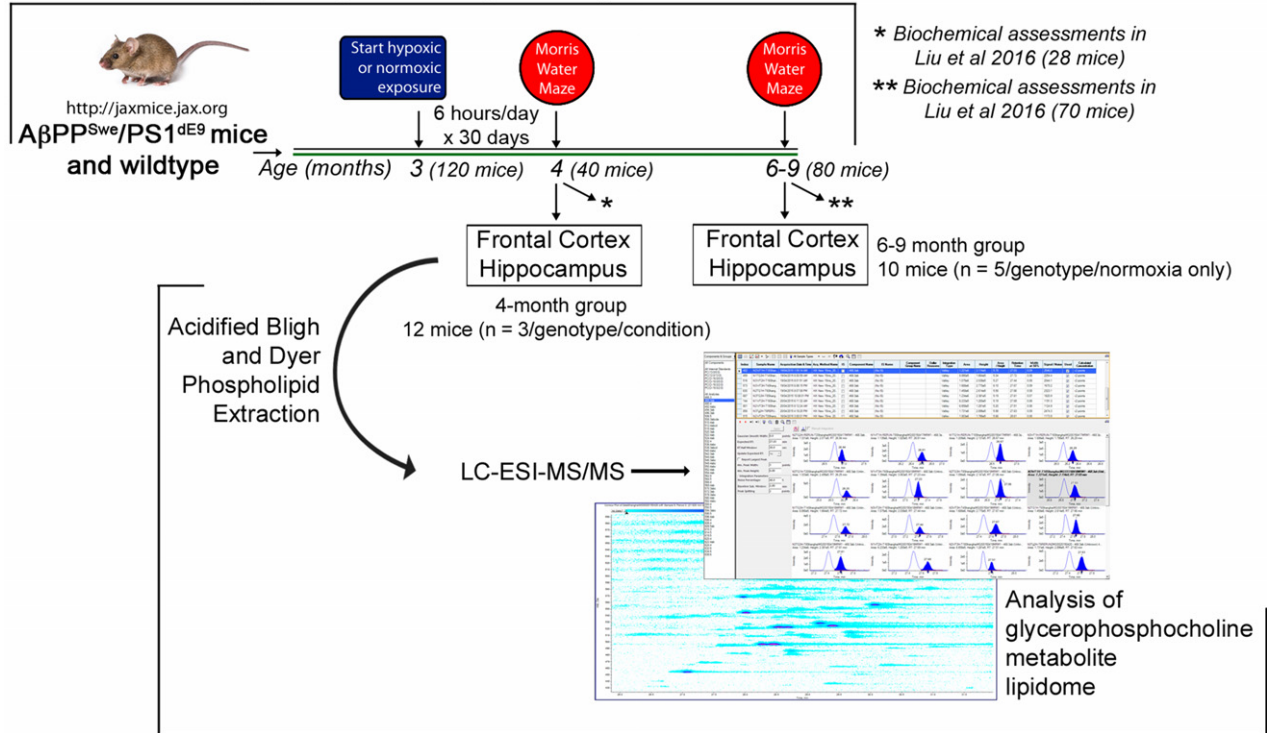
Animals

A β PP^{Swe}/PSI^{dE9} mice (004462; Jackson Laboratories, Bar Harbor, MA, USA, RRID:SCR_000708) on a F2 C57BL/6J X C3H/HeJ background were bred to C57BL/6J (000664; Jackson Laboratories, RRID:SCR_000708) mice in the Le laboratory. A flowchart of our experimental paradigm is presented in Fig. 1. A total of $n = 120$ littermates (60 males and 60 females) were randomly assigned to control (normoxic) or hypoxic treatment at 3 months of age using a random number generator. Because one of our prerequisites before randomization was that our experimental groups contained equal numbers of animals, this randomization process is referred to as pseudo-randomization. Full treatment details and all of the behavioral results for the mice profiled in this study ($n = 22$ of $n = 120$) can be found in Liu *et al.* (2016). Briefly, A β PP^{Swe}/PSI^{dE9} and wild-type (WT) littermates were placed in a hypobaric chamber and exposed to either hypoxic or normoxic conditions for 6 h/day for 30 consecutive days at 3 months of age. Experimenters were blinded as to the genotype of the animals over the course of treatment. In the hypoxic group, oxygen levels were reduced to 11.1% to simulate a high-altitude hypoxia of approximately 5000 meters high. In the normoxic group, animals were handled and exposed to the same chambers for equivalent periods of time under normobaric conditions. Water and food (Xietong Medical Biological Engineering, 1010009) were available *ad libitum*. Following a 1-month schedule of chronic intermittent hypoxia or sham (normoxic) treatment, mice were divided into three cohorts using the same pseudo-randomization methodology described above ($n = 10$ /genotype/normoxic or hypoxic conditions). Mice were

tested using the Morris Water Maze (MWM) at 4, 6, and 9 months of age by an experimenter blinded as to the genotype and treatment of each mouse. Animals were sacrificed within 3 days of testing. At the time of sacrifice, mice were again pseudo-randomly assigned using a random number generator for the biochemical assessments ($n = 98$) reported in Liu *et al.* (2016) or the lipidomic assessments described here ($n = 22$). A total of twelve 4-month-old mice ($n = 3$ /genotype/normoxic or hypoxic condition) and ten 6- to 9-month-old mice ($n = 5$ /genotype/normoxic manipulation only) were analyzed. All lipidomic analyses were performed by an experimenter blinded to the genotype and performance of each mouse on the MWM. Frontal cortex, composed of the frontal association cortex and primary and secondary motor cortices, between bregma 3.20 and 2.46, and hippocampi between bregma -0.82 and -4.16 were dissected bilaterally on ice using a Zeiss Axio Zoom dissecting scope (Fig. 2), weighed, flash-frozen in liquid nitrogen at the time of sacrifice, and maintained at -80°C until lipid extraction. Sample sizes indicate biological replicates (number of mice) of each brain region analyzed. All protocols were performed according to Laboratory Animal Care Guidelines and sanctioned by the Animal Committee of Shanghai Jiao Tong University School of Medicine. We had no pre-determined inclusion or exclusion criteria for the behavioral experiments; all animals tested were included.

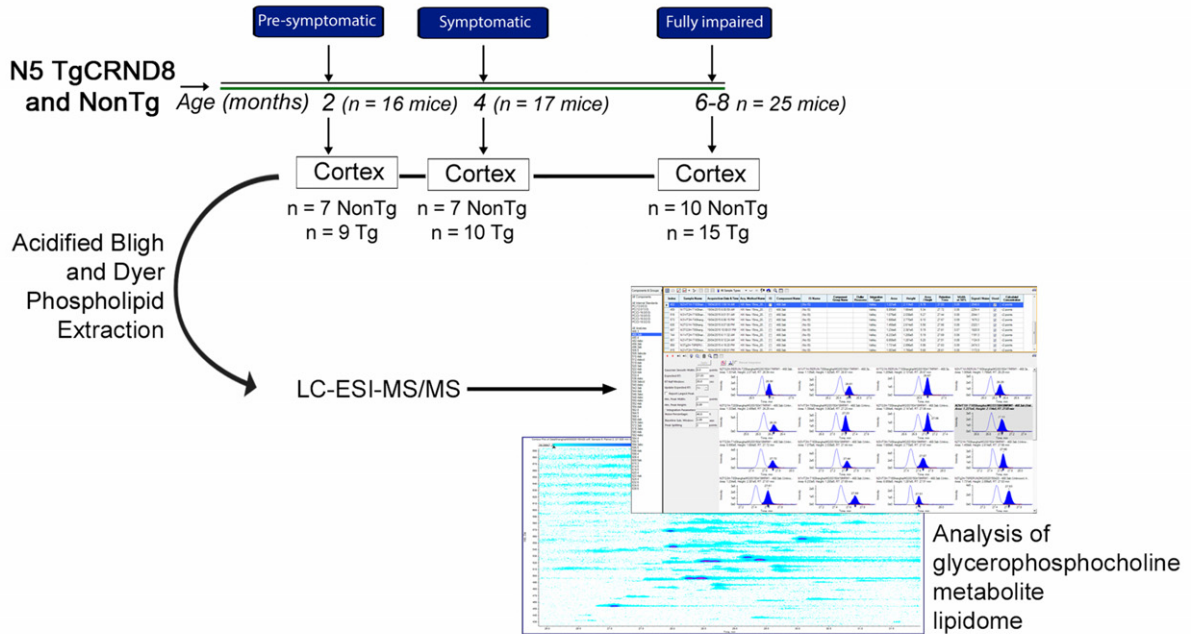
A total of 58 female N5 TgCRND8 (Tg) and (Non-Tg) littermates were randomly assigned using a random number generator at time of weaning for assessment at 2 ($n = 9$ Tg; $n = 7$ Non-Tg), 4 ($n = 10$ Tg; $n = 7$ Non-Tg), 6 ($n = 9$ Tg; $n = 7$ Non-Tg), and 8 ($n = 6$ Tg; $n = 3$ Non-Tg) months of age. Water and food (Envigo, Mississauga, ON, Canada, 2018 Teklad Global 18% Protein Rodent Diet) were available *ad libitum*. N5 TgCRND8 (RRID:SCR_000708) mice are a subline of the C57BL/6J X C3H/HeJ TgCRND8 mouse model (Chishti *et al.* 2001) back-crossed in the Bennett laboratory for five generations (N5) to a C57BL/6Ncrl lineage and maintained by sibling crosses (Granger *et al.* 2016). This line does not carry the parental *Pde6b*^{rd1} retinal degeneration mutation that renders homozygotes blind (Chang *et al.* 2002) or the *Nnt*^{C57BL/6J} allele responsible for diminished insulin secretion and impaired glucose tolerance (Toye *et al.* 2005). We have previously shown that female N5 Tg mice are pre-symptomatic at 2 months of age, start to show behavioral impairments in the MWM at 4 months of age, and are maximally impaired at 6 months of age (Wang *et al.* 2013; Granger *et al.* 2016). Learning and memory deficits are observed for at least 12 months of age (Wang *et al.* 2013; Granger *et al.* 2016). Temporal-parietal-entorhinal cortices, referred to as cortex, composed of primary somatosensory, parietal and parietal association, primary and secondary visual, retrosplenial granular, secondary audiovisual, temporal association, entorhinal, perirhinal, entorhinal, and piriform cortices between bregma -0.82 and -4.16 , were dissected bilaterally on ice using a Leica MZ6 dissecting scope (Fig. 2), weighed, flash-frozen in liquid nitrogen at the time of sacrifice, and maintained at -80°C until extraction. Quantification of lipid abundances was performed by experimenters blinded as to the genotype and age of the mice. All procedures were approved by the Animal Care Committee of the University of Ottawa and performed in strict accordance with the ethical guidelines for experimentation of the Canadian Council for Animal Care. These studies were not pre-registered.

(a) Institute of Neurology, Shanghai Jiao Tong University School of Medicine



Neural Regeneration Laboratory, India Taylor Lipidomics Research Platform, University of Ottawa

(b)



Neural Regeneration Laboratory, India Taylor Lipidomics Research Platform, University of Ottawa

Phospholipid extractions

Dissected brain tissues were extracted using modified Bligh and Dyer protocol (Bligh and Dyer 1959) previously described (Xu *et al.* 2013). Briefly, tissues were homogenized using a tissue tearer (985370; BioSpec, Bartlesville, OK, USA) in 4 mL acidified

methanol (A412P-4; Fisher, RRID:SCR_003374) containing 2% acetic acid (351271-212; Fisher, Nepean, ON, Canada, RRID:SCR_003374). MS grade lipid standards, PC(13:0/0:0) [90.7 ng Avanti LM-1600] and PC(12:0/13:0) [100 ng, LM-1000; Avanti, Alabaster, AL, USA], were added to the homogenate at the time of

Fig. 1 Flowchart of our experimental paradigm. (a) In this study, A β PP^{Swe}/PS1^{DE9} mice and WT littermate controls bred at the Institute of Neurology in the Shanghai Jiao Tong University of Medicine, were subjected to either hypoxic or normoxic (sham) treatment in a hypobaric chamber for 6 h/day for 30 days between 3 and 4 months of age at the Institute of Neurology in the Shanghai Jiao Tong University of Medicine. Separate cohorts of mice subsequently underwent MWM testing for learning and memory at either 4 or 6–9 months of age. Their performance in this test has been published in Liu *et al.* (2016). Mice were sacrificed after MWM testing, frontal cortices and hippocampi

were dissected and transferred to the Neural Regeneration Laboratory at the University of Ottawa for glycerophospholipid extraction and lipidomic analyses. (b) N5 TgCRND8 mice, bred in the Neural Regeneration Laboratory at the University of Ottawa were sacrificed at 2, 4, and 6–8 months of age whereupon temporal/parietal/entorhinal cortices were dissected and underwent the same glycerophospholipid and lipidomic analysis of glycerophosphocholine second messengers and metabolites as A β PP^{Swe}/PS1^{DE9} mice. A β PP, amyloid precursor protein; MWM, Morris Water Maze.

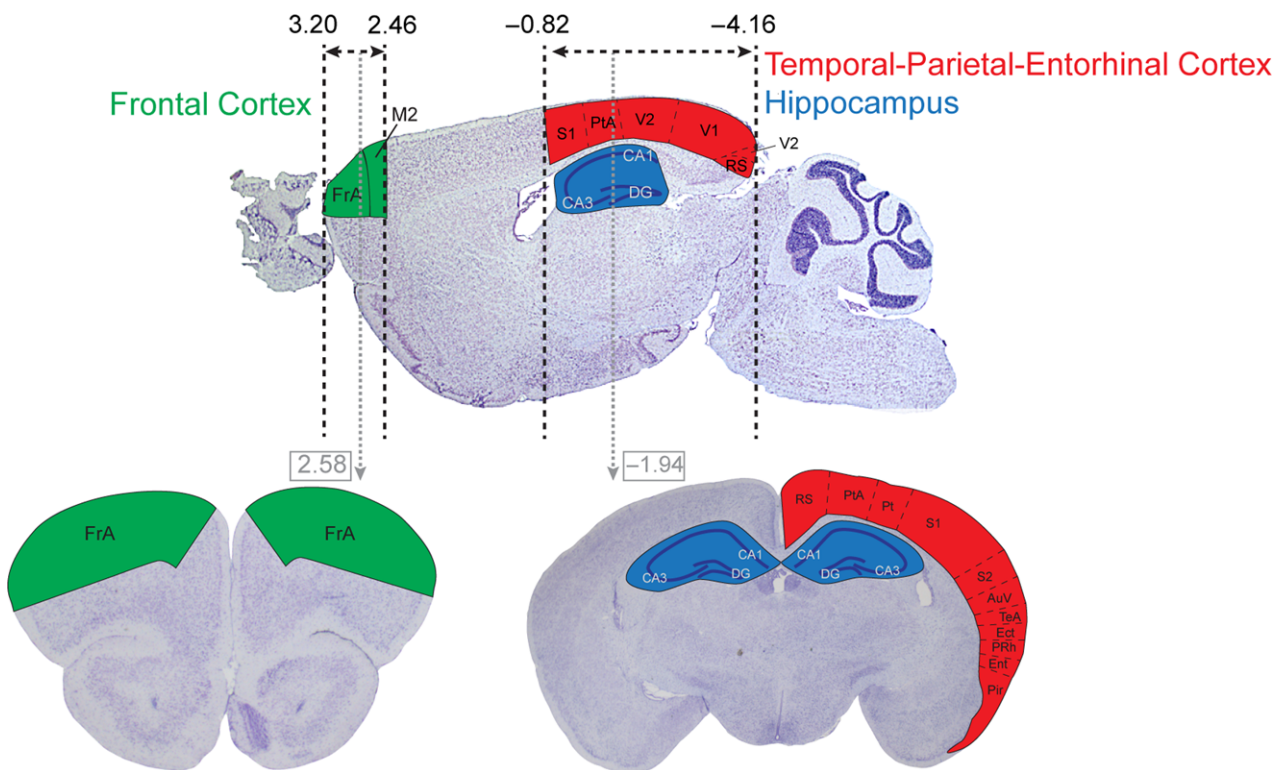


Fig. 2 Schematic of dissections and regions profiled by LC-ESI-MS/MS. Frontal cortex, comprising the frontal association cortex and part of the secondary motor cortex between bregma 3.2 and 2.46, and hippocampus (dorsal and ventral) between bregma -0.82 and -4.16 were dissected from WT and A β PP^{Swe}/PS1^{DE9} mice. Temporal/Parietal/Entorhinal cortices comprising the primary somatosensory, parietal and parietal association, primary and secondary visual, retrosplenial granular, secondary audiovisual, temporal association, entorhinal, perirhinal, entorhinal, and piriform cortices between bregma -0.82 and -4.16 were dissected from Non-Tg and Tg mice.

Abbreviations: AuV, secondary audiovisual cortex; CA1, Cornu Ammonis field 1 of the hippocampus; CA3, Cornu Ammonis field 3 of the hippocampus; DG, dentate gyrus; Ect, entorhinal cortex; Ent, entorhinal cortex; FrA, frontal association cortex; M2, secondary motor cortex; Pir, Piriform cortex; PRh, perirhinal cortex; Pt, parietal cortex; PtA, parietal association cortex; RS, retrosplenial granular cortex; S1, primary somatosensory cortex; TeA, temporal association cortex; V1, primary visual cortex; V2 secondary visual cortex; A β PP, amyloid-beta precursor protein.

extraction. Chloroform (C298-500; Fisher, RRID:SCR_003374) and 0.1 M sodium acetate (S-2889; Sigma-Aldrich, Oakville, ON, Canada, RRID:SCR_008988) were added to each sample at a final ratio of acidified methanol/chloroform/sodium acetate of 2 : 1.9 : 1.6. Samples were vortexed and centrifuged at 600 g for 10 min at 4°C. The organic phase was retained and the aqueous phase successively back-extracted using chloroform. The four organic extracts were combined and evaporated at 22°C under a constant stream of nitrogen gas. Final extracts were solubilized

in 300 μ L of anhydrous ethanol (P016EAAN; Commercial Alcohols, Toronto, ON, Canada) and stored under nitrogen gas at -80°C in amber vials (C779100AW; BioLynx, Brockville, ON, Canada).

High-performance liquid chromatography electrospray ionization tandem mass spectrometry (HPLC-ESI-MS/MS)

HPLC was performed using an Agilent 1100 system with an autosampler maintained at 4°C. Samples were prepared for LC

injection by mixing 5 μL of lipid extract with 2.5 μL of an internal standard mixture consisting of PC(O-16:0-d₄/0:0) [2.5 ng, 360906; Cayman, Ann Arbor, MI, USA, RRID:SCR_008945], PC(O-18:0-d₄/0:0) [2.5 ng, 10010228; Cayman, RRID:SCR_008945], PC(O-16:0-d₄/2:0) [1.25 ng, 360900; Cayman, RRID:SCR_008945], and PC(O-18:0-d₄/2:0) [1.25 ng, 10010229; Cayman, RRID:SCR_008945] in EtOH, and 16 μL of Solvent A (see below). Chromatography was performed on a 12 cm \times 75 μm (I.D.) column packed with ReproSil-Pur 120 C4 (particle size of 5 μm and pore size of 120 Å , Dr. A. Maisch, Ammerbruch, Germany #r15.4e) with a binary solvent gradient of water with 0.1% formic acid and 10 mM ammonium acetate (Solvent A) and acetonitrile/isopropanol (5 : 2 v/v) with 0.1% formic acid and 10 mM ammonium acetate (Solvent B). Solvents were pumped at a main flow of 20 $\mu\text{L}/\text{min}$ and a split flow configuration was used to achieve submicroliter/minute flow rate. The gradient started at 5% B, held for 15 min, was then increased to 100% B over 5 min, and was maintained for 25 min for column re-equilibration. The solvent composition was brought back to 5% B within 1 min and maintained for 15 min. Each sample injection was followed by a blank run to ensure no significant carryover. MS acquisition was performed using a QTRAP 5500 system equipped with a NanoSpray III ion source (SCIEX) with the following optimized instrument parameters: curtain gas was set to 20 $\mu\text{L}/\text{min}$; ion spray voltage to 2500 V, and source gas to 10 $\mu\text{L}/\text{min}$. LC-MS protocols were optimized as follows to ensure sensitivity in the quantification of low abundant lipid metabolites and second messengers.

The complete glycerophosphocholine-containing metabolome (450–650 m/z) in the frontal cortex, temporal/parietal/entorhinal cortex, and hippocampus was profiled using precursor ion scan (PIS) in positive ion mode monitoring the diagnostic product ion of the glycerophosphocholine headgroup at m/z 184.1. To differentiate *lysosphingomyelins* and *sphingomyelins* from glycerophosphocholines with the same headgroup, we used differential mobility spectroscopy (DMS)-based experiments on a QTRAP 5500 mass spectrometer equipped with SelexION DMS technology (SCIEX) and a Turbo V ion source (SCIEX, Concord, ON, Canada). Operating conditions were optimized using a lipid standard mixture containing 1 μM PC(12:0/13:0) (LM-1000; Avanti) and porcine brain SM (860062; Avanti) with 1-propanol as the DMS chemical modifier. The lipid standards were T-infused with an integrated syringe pump set at 5 $\mu\text{L}/\text{min}$ into the flow of 10 $\mu\text{L}/\text{min}$ of 100% Solvent B (acetonitrile/isopropanol at 5 : 2 v/v ratio containing 0.1% formic acid and 10 mM ammonium acetate) delivered by an Agilent Infinity II system (RRID:SCR_013575; Agilent, Mississauga, ON, Canada). The optimized DMS conditions were as follows: separation voltage = 3900 V, DMS cell temperature = 150°C (Low), modifier concentration = 1.5% v/v in the transport gas (Low), DMS resolution enhancement = 18 psi (Low), and DMS offset = -3.0 V. The compensation voltage (COV) values were then optimized for each lipid class by ramping the COV at increments of 0.1 V and the optimal COV values for glycerophosphocholines and sphingomyelins were determined to be -4.5 V and 1.5 V, respectively. For the flow injection-DMS experiments, the species within each lipid class were monitored using (+) Prec184 for glycerophosphocholines and sphingomyelins with the pre-determined optimal COV values.

Quantitative analysis of validated glycerophosphocholine metabolites and second messengers detected in our profiles was

achieved in selected reaction monitoring (SRM) mode monitoring the transition from the protonated molecular ion of each of the lipid species detected to the headgroup specific product ion of m/z 184.1. Collision gas was set to 10 $\mu\text{L}/\text{min}$ with an entrance potential of 10 eV, a declustering potential of 100 eV, and a collision cell exit potential of 9 eV. Collision energy was 47 eV. PIS and SRM spectra were analyzed using Analyst 1.6.2 and MultiQuant 3.0.8664.0 (SCIEX), respectively. Analysis output was converted to .csv format for further bioinformatic processing. Spectra were aligned using RT-STAR (v1.0), an in-house algorithm that standardizes retention times to align lipid species across lipidomes. Molecular identities were assigned using ValID v3.0 (Blanchard *et al.* 2013) and the LIPID MAPS Structural Database (RRID:SCR_003817) (Sud *et al.* 2007). Molecular identities were confirmed in a single HPLC-SRM- information dependent acquisition (IDA)- enhanced product ion (EPI) experiment in which SRM was used as a survey scan to identify target analytes and an IDA of EPI spectra were acquired in the linear ion trap. After acquisition, the EPI spectra were examined for structural determination. For quantification, raw peak areas were corrected for extraction efficiency and instrument response by normalization to internal standards, PC(12:0/13:0) or PC(13:0/0:0), added at the time of extraction. Lipid abundances were expressed as pmol equivalent of internal standard per mg of tissue wet weight (pmol/mg_{tissue}) or as log₂ fold change in these abundances relative to control.

Lipid nomenclature

We used the standard lipid nomenclature described by Fahy *et al.*, to identify individual lipids (Fahy *et al.* 2011). For example, PC(O-18:1/2:0) defines a molecular species belonging to the glycerophosphocholine class of lipids with a polar phosphocholine head group (PC) at the *sn*-3 position of the glycerol backbone, a hydrocarbon chain of 18 carbons with 1 double bond at the *sn*-1 position via an alkyl (ether) linkage (O-), and a saturated fatty acyl chain of 2 carbons at the *sn*-2 position via an ester linkage. For other subclasses, the nomenclature P- refers to an alkenyl (vinyl ether) linkage at the *sn*-1 position. Lack of linkage indicators refers to an acyl (ester) linkage. PC(O)-PAF second messengers were defined by their acetyl group at the *sn*-2 position. PAF-like lipids were defined as having an *sn*-1 acyl-group (PC-PAF) or alkenyl-group (PC(P)-PAF) and up to 2–6 carbons at the *sn*-2 position. We profiled LPC, LPC(O), and LPC(P) as well as PC(O)-PAF and PAF-like PC-PAF and PC(P)-PAF metabolites and second messengers (Supplemental Figure S1).

Western analyses

Cortices were homogenized in Urea-Tris (8 M Urea, 50 mM Tris pH 8.2, 65 mM dithiothreitol [#U5128, #T1503, and #43815; Sigma-Aldrich] supplemented with EDTA-free protease inhibitor and phosphatase inhibitor cocktail tablets [#04693124001 and #04906837001; Roche Molecular Biochemicals, Indianapolis, IN, USA] and sonicated (#Sonicator3000; QSonica, Newton, CT, USA) three times at 12 W for 20 s. The samples were passed through a 26-gauge needle (#309625; BD Biosciences, Mississauga, ON, Canada) eight times and centrifuged at 22 000 g for 15 min. Protein concentrations were assessed using the Bio-Rad DC protein assay kit (#500-0112; Bio-Rad Laboratories, Hercules, CA, USA). Protein was denatured using the NuPAGE LDS sample buffer and reducing agent (#NP0007, and #NP0009; Life

Technologies, Grand Island, NY, USA) in accordance to the manufacturer's guidelines. Thirty μg of protein per well were resolved on NuPAGE 4–12% sodium dodecyl sulfate–polyacrylamide gel electrophoresis gels (#NP0335; Life Technologies). Gels were transferred onto nitrocellulose membranes (#66485; Pall Corporation, Portland, NY, USA) and blocked for 30 min with Phosphate Buffered Saline-Tween (PBS-T) (Phosphate-Buffered Saline-Tween: 10 mM phosphate pH 7.2, 154 mM NaCl [#SPD307, #SPM306, and #SOD001; BioShop, Burlington, ON, Canada], 0.1% (v/v) Tween 20 [#P1379; Sigma-Aldrich]) containing 5% (w/v) non-fat milk (Nestle Carnation, Arlington, VA, USA). Membranes were incubated at 4°C overnight with the primary antibody in PBS-T with 3% (w/v) non-fat milk. Primary antibodies were anti-PAFAH1B1 (LIS1, 1 : 1000, RRID: AB 10694968, #AB5413; Millipore Corporation, Bedford, MA, USA), anti-PAFAH1B2 (α_2 , 1 : 700, gift of Dr Arai, University of Tokyo), anti-PAFAH1B3 (α_1 , 1 : 700, gift of Dr Arai), and anti-actin (#CLT9001; Cedarlane, Burlington, ON, Canada). Horseradish peroxidase-conjugated anti-mouse (1 : 2000, #610-1319-0500, 1 : 2000; Rockland, Limerick, PA, USA) or anti-rabbit IgG (1 : 5000, #NA834V; GE Healthcare, Chicago, IL, USA) secondary antibodies in 3% (w/v) non-fat milk PBS-T were incubated with the membranes for 1 h at 22°C. Reactions were visualized using Immobilon Western Chemiluminescent HRP Substrate (#WBKLS0500; Millipore Corporation). Membranes were stripped using 1 \times ReBlot plus solution (#2504; Millipore Corporation) according to the manufacturer's guidelines. Relative protein expression was quantified by densitometry using the image processing program Fiji v1.0 (National Institutes of Health).

PLA₂ α activity

Total Group IV cPLA₂ α activity was assessed in cortical lysates using a commercial assay kit (#765021; Cayman) according to manufacturer's guidelines.

Statistics

Statistical analyses were performed using Prism 7.0d (GraphPad Software Inc., San Diego, CA, USA, RRID:SCR_002798). An alpha value of $p < 0.05$ was deemed statistically significant. *Post hoc* power analyses were performed for all significant effects using G*Power 3.1 (RRID:SCR_013726) (Faul *et al.* 2007) with α set to 0.05. Sample and effect sizes were deemed acceptable maintaining a β value of 0.2 or under. Univariate analyses were unpaired, two-tailed *t*-tests and one- or two-way ANOVAs as indicated. In the event of multiple *t*-tests, family-wise error was corrected for by setting the false discovery rate to $Q = 0.05$ according to the method of Benjamini *et al.* (2006). In ANOVA analyses, Holm–Sidak *post hoc* tests were used to control for family-wise comparisons. In multivariate assessments, autoscaled pmol equivalents per mg tissue wet weight reflecting the number of standard deviations each sample fell from the mean abundance of each lipid species were subjected to partial least squares-discriminant analysis and variable importance in projection scores were calculated using MetaboAnalyst 3.0 (RRID:SCR_015539) (Xia *et al.* 2015). Where a lipid species was below our limits of quantification, missing values were estimated as twofold less than the lowest lipid abundance in all samples. Average linkage hierarchical clustering using city-block similarity metrics (autoscaled pmol equivalents per mg tissue wet weight) or

uncentered correlation metrics (\log_2 fold changes) were performed using Cluster 3.0 (RRID:SCR_013505) (de Hoon *et al.* 2004). Heatmaps were visualized using Java TreeView 1.1.6 (RRID:SCR_013503) (Saldanha 2004).

Results

The cortical and hippocampal glycerophosphocholine metabolite lipidomes are distinct

We first identified the repertoire of glycerophosphocholine metabolites and second messengers with *m/z* between 450 and 650 in the frontal cortex and hippocampus of adult 4- to 9-month-old WT mice using HPLC-ESI-MS/MS by PIS in positive ion mode. Because these species are much less abundant than their structural precursors, we developed and optimized a nano-flow HPLC-ESI-MS/MS method using a NanoSpray III ion source for their detection and quantification. Dynamic range of detection was confirmed by serial dilution and abundances of all species reported in this study were within this dynamic range. Our analysis excluded sphingomyelins and *lyso*-sphingomyelins identified by HPLC-DMS-ESI-MS/MS (Supplemental Figure S2). Molecular identities were confirmed in a single HPLC-SRM-IDA-EPI experiment.

A total of 61 lipids were profiled as Land's cycle metabolites and second messengers. Cortical and hippocampal metabolite lipidomes segregated according to lipid composition and species abundance (Fig. 3a). Four species were unique to the frontal cortex: one PC-PAF-like lipid, PC(18:1/3:0), two LPC(O), LPC(O-18:0/0:0) and LPC(O-21:6/0:0), and one PC(O)-PAF, PC(O-17:0/2:0) (Fig. 3a and b). Eight species were unique to the hippocampus: one PC-PAF, PC(16:0/2:0) and one PC-PAF-like lipid, PC(18:1/4:0); four LPCs, LPC(26:6/0:0), LPC(22:6/0:0), LPC(22:4/0:0), and LPC(19:1/0:0); one PC(O)-PAF, PC(O-17:1/2:0); and one LPC(P), LPC(P-20:0/0:0) (Fig. 3a and b). The most abundant glycerophosphocholine metabolites in both regions were LPC(18:0/0:0) and LPC(16:0/0:0), making up 40% mol of the total metabolite lipidome. There were no regional differences in the abundances of these species; consequently, there were no statistically significant regional differences in total lipid metabolite content (Fig. 3c and d). Overall levels of PC(O)-PAF and LPC(P) were, however, lower in cortex compared to hippocampus (Fig. 3c). At the molecular level, abundances of 21 LPC, LPC(O), PC(P)-PAF, and PC(O)-PAF species were lower in the frontal cortex compared to the hippocampus (Fig. 3d).

Glycerophosphocholine metabolism is disrupted in the frontal cortex but not the hippocampus of A β PP^{Swe}/PS1^{dE9} mice when older mice transition from a pre-symptomatic to a symptomatic state

The A β PP^{Swe}/PS1^{dE9} mice used in this study were a randomly chosen subset of animals previously subjected to normoxic or hypoxic challenge (Liu *et al.* 2016). All of

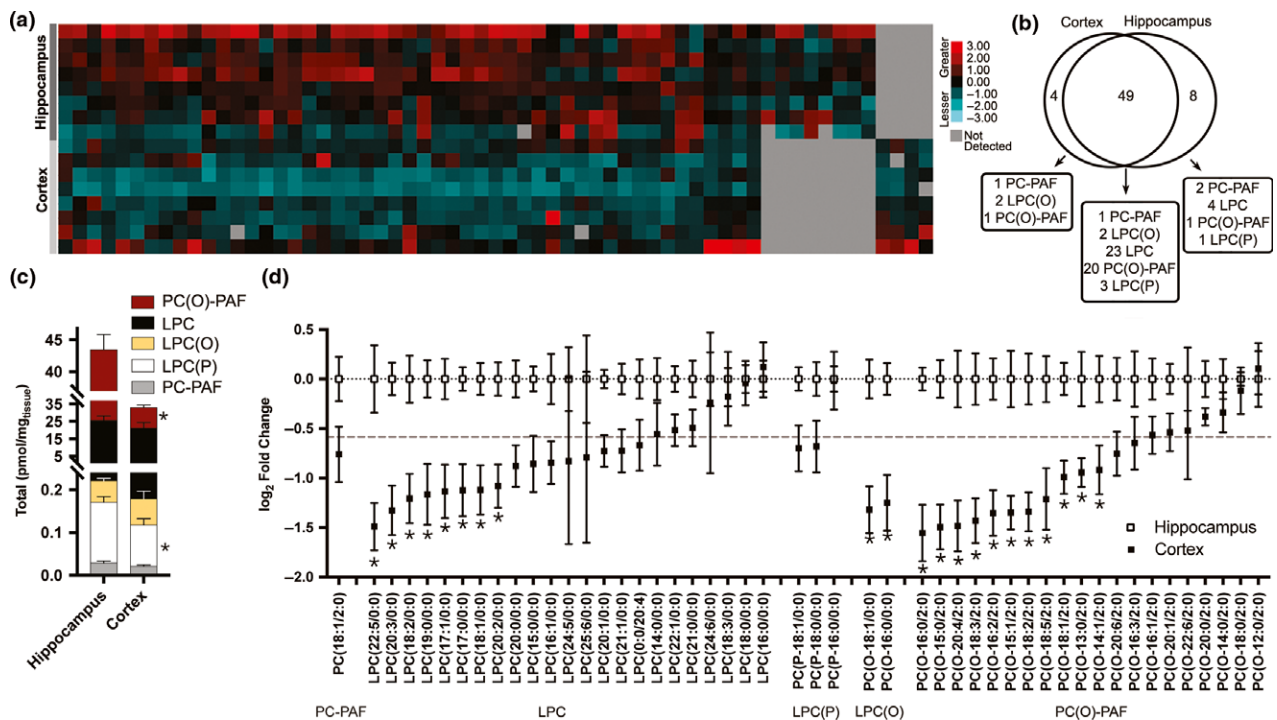


Fig. 3 Cortical and hippocampal glycerophosphocholine metabolite lipidomes are distinct. (a) Heatmap depicting separation of the cortical and hippocampal glycerophosphocholine metabolite and second messenger landscapes. Data represent autoscaled metabolite abundances calculated in pmol per mg tissue wet weight) of adult (4–8-month-old, $n = 8$) normoxic-treated WT mice. Z-scores were clustered using average linkage hierarchical clustering according to city-block similarity metrics. Legend indicates number of standard deviations each value follows from the overall mean. (b) Venn diagram summarizing glycerophosphocholine metabolite composition in frontal cortex and hippocampus. (c) Total glycerophosphocholine metabolite and second messenger abundances were comparable across regions; subclass abundances of LPC(P) and PC

(O) were lower in cortex compared to hippocampus. Data represent lipid abundance in pmol per mg tissue wet weight \pm standard error (SEM). Statistics were multiple t -tests corrected for multiple comparisons by false discovery rate (FDR) with $Q = 0.05$. LPC(P): two-tailed unpaired $t = 2.30$, $df = 14$, $q = 0.037$; PC(O)-PAF: $t = 2.15$, $df = 14$, $q = 0.049$. * $Q < 0.05$. (d) Differences in regional metabolite abundance were species specific. Data depict mean \log_2 fold change \pm SEM ($n = 8$ animals). Each sample was divided by the average abundance of the same lipid species in the hippocampus. Statistics were multiple unpaired t -tests with an FDR of 5%; *FDR-adjusted $Q < 0.05$. LPC(P), monoalkenylglycerophosphocholine; PC (O), monoalkylglycerophosphocholine

the behavioral data for these animals are presented in (Liu *et al.* 2016) as are the cortical levels of A β . In Liu *et al.* (2016), we demonstrated that the performance of normoxic-treated WT animals was comparable in the MWM at 4, 6, and 9 months of age. Animals showed no learning and memory deficits. Likewise, we found here that their glycerophosphocholine lipidomes were indistinguishable. Total abundances of PC-PAF, LPC, LPC(P), LPC(O), and PC(O)-PAF did not change between 4 and 9 months of age (Fig. 4a). Next, we compared the lipidomes of pre-symptomatic A β PP^{Swe}/PS1^{DE9} mice to their WT littermates at 4 months of age. There were no differences in lipid abundances prior to symptomatic onset (Supplemental Table S1). Finally, we interrogated the lipidomes of normoxic A β PP^{Swe}/PS1^{DE9} mice before (pre-symptomatic 4-month-old mice) and after (symptomatic 6- to 9-month old mice) the onset of learning and memory impairment.

We found that LPC levels were significantly lower in older symptomatic compared with younger pre-symptomatic A β PP^{Swe}/PS1^{DE9} mice (Fig. 4b).

Chronic intermittent hypoxia accelerates changes in cortical glycerophosphocholine metabolism associated with symptomatic onset in A β PP^{Swe}/PS1^{DE9} mice

We used multivariate partial least squares-discriminant analysis to determine whether the glycerophosphocholine metabolite lipidome discriminated pre-symptomatic from post-symptomatic A β PP^{Swe}/PS1^{DE9} mice. Pre-symptomatic young mice clearly segregated from symptomatic older mice using the first two principal components in two-dimensional score plots (Fig. 5a, left panel). In Liu *et al.* (2016), we reported that exposure to chronic intermittent hypoxia accelerated A β PP^{Swe}/PS1^{DE9} phenotypic conversion. The hypoxic A β PP^{Swe}/PS1^{DE9} mice profiled here showed learning and

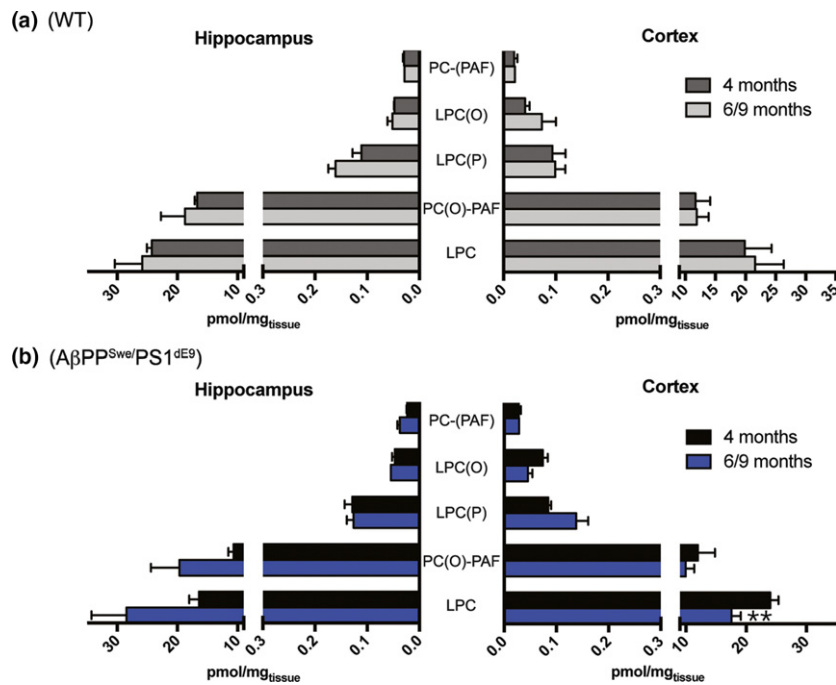


Fig. 4 The cortical but not hippocampal lipidome is altered when AβPP^{Swe}/PS1^{dE9} mice first exhibit learning and memory deficits. (a) No statistically significant age-related changes in glycerophosphocholine metabolite levels were detected in normoxic WT mice at 4 months compared to 6- and 9-month-old mice in either the hippocampus or the cortex. There was also no difference in the hippocampal or cortical lipidomes of WT or pre-symptomatic AβPP^{Swe}/PS1^{dE9} mice at 4 months of age (data presented in Supplemental Table S1). (b)

Cortical levels of *lyso*-phosphatidylcholines (LPCs) significantly decreased at symptomatic onset in AβPP^{Swe}/PS1^{dE9} mice under normoxic conditions. No changes in glycerophosphocholine metabolite levels were detected in the hippocampus. Data represent mean lipid abundance (pmol per mg tissue wet weight) ± SEM. Statistics were two-way ANOVA with a significant main effect of age ($F_{(1,30)} = 5.1$, $p = 0.03$) with Holm-Sidak *post hoc* tests for multiple comparisons (** $p < 0.01$). AβPP, amyloid precursor protein.

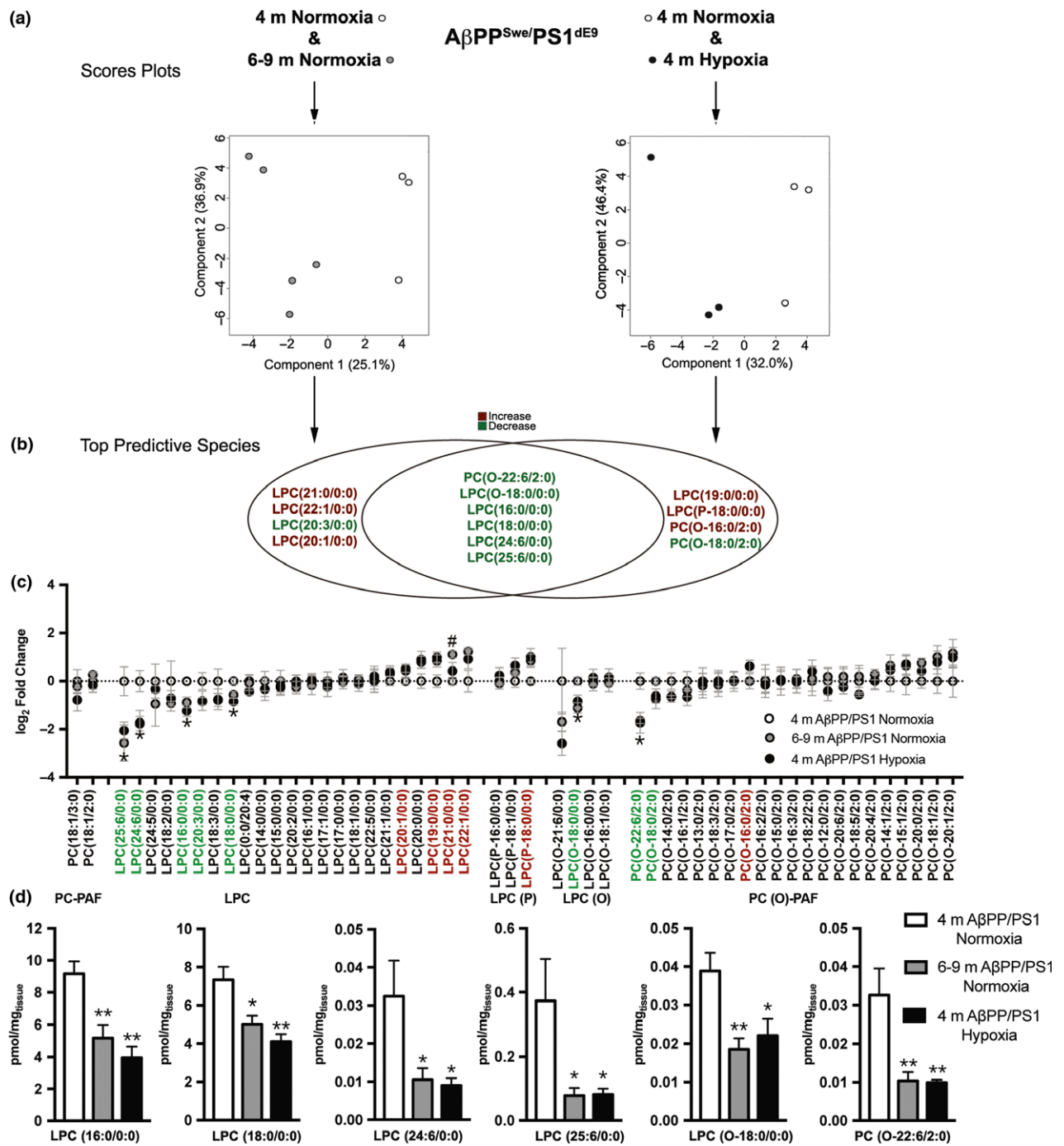
memory deficits by 4 months of age; normoxic AβPP^{Swe}/PS1^{dE9} mice phenoconverted between 6 and 9 months of age (Liu *et al.* 2016). We found that these same pre-symptomatic normoxic 4-month-old AβPP^{Swe}/PS1^{dE9} mice were also clearly discriminated from symptomatic hypoxic 4-month-old littermates (Fig. 5a, right panel).

We next asked whether age- and hypoxia-induced phenoconversion elicited the same changes in cortical lipid metabolism. Sixty percent of the top 10 critical discriminators of age- and hypoxia-induced phenoconversion were identical (Fig. 5b). These lipids also showed statistically significant decreases relative to normoxic 4-month-old pre-symptomatic mice (Fig. 5c). Lipid abundances of five glycerophosphocholine metabolites, LPC(16:0/0:0), LPC(18:0/0:0), LPC(24:6/0:0), LPC(25:6/0:0), LPC(O-18:0/0:0), and PC(O-22:6/2:0) declined significantly in both age-dependent and hypoxia-induced symptomatic AβPP^{Swe}/PS1^{dE9} but not WT mice (Fig. 5d, Supplemental Table S1). Hypoxia did not significantly alter the WT lipidome (Supplemental Figure S3). Levels of five of the six critical indicators of AβPP^{Swe}/PS1^{dE9} phenoconversion declined mildly in WT littermates following hypoxic challenge;

however, none of these changes were statistically significant (Supplemental Figure S3). Taken together, these data suggested that PLA₂ activity is reduced when AβPP^{Swe}/PS1^{dE9} mice first exhibit either age- or environmental risk-associated learning and memory deficits.

Changes in PLA₂ activity and PAFAH1b subunit protein expression mark symptomatic onset and symptomatic progression in N5 TgCRND8 mice

To assess enzymatic levels, activity, and lipidomic impact directly, we profiled the Land's cycle glycerophosphocholine metabolome and associated enzyme activities/levels in a second AβPP mouse model. N5 TgCRND9 mice (Granger *et al.* 2016) are a TgCRND8 subline, expressing the human AβPP gene with Swedish and Indiana familial AD mutations (KM670/671NL+V717F) under the control of the prion protein promoter (Chishti *et al.* 2001). N5 TgCRND8 females (Tg) are pre-symptomatic at 2 months of age, phenoconvert in the MWM between 4 and 5 months, and are fully impaired at 6 months of age with deficits tested up to 12 months of age (Wang *et al.* 2013; Granger *et al.* 2016). Aβ-plaques are observed by 4 months of age and the



$A\beta_{2/40}$ ratio exceeds unity by 6 months of age (Granger et al. 2016). We quantified Land's cycle metabolites and second messengers in the temporal/parietal/entorhinal cortex of 2- (pre-symptomatic), 4- (onset of learning and memory deficits), 6- (fully impaired), and 8- (fully impaired) month-old Tg mice by LC-ESI-MS/MS (Fig. 6a). As observed in the frontal cortex of $A\beta_{PP}^{Swe}/PS1^{dE9}$ mice, overall abundances of LPC metabolites decreased significantly when 4-

month-old Tg mice first exhibited learning and memory deficits (Fig. 6a and b). In addition, significant decreases in LPC(O) metabolites were detected (Fig. 6a and b). In older 6- and 8-month-old mice, total LPC and LPC(O) levels rebounded (Fig. 6a and b) and PC(O)-PAF levels rose (Fig. 6a and c). We compared product to precursor ratios of PC(O-18:1/2:0) to LPC(O-18:1/0:0) to assess the rate of conversion of *lyso*-PAF to PAFs in both Tg and wild-type

Fig. 5 Chronic hypoxia accelerates glycerophosphocholine metabolic changes associated with the onset of behavioral impairment in the cortex of A β PP^{Swe}/PS1^{dE9} but not WT mice. (a) PLS-DA score plots demonstrating distinct separation of impaired A β PP^{Swe}/PS1^{dE9} 6–9-month normoxic (left panel) and 4-month hypoxic (right panel) mice from pre-symptomatic A β PP^{Swe}/PS1^{dE9} mice. (b) A Venn diagram depicting the top 10 critical glycerophosphocholine metabolites identified by PLS-DA analysis with the highest variable projection score (all ≥ 1.4). Of these, six species were common in discriminating phenocconversion of both older normoxic (left ellipse) and younger hypoxic (right ellipse) A β PP^{Swe}/PS1^{dE9} mice. Red font indicates increased abundance in symptomatic mice, green font indicates decreased abundance in symptomatic mice. (c) Levels of these six critical predictors of symptomatic onset were statistically significantly lower following phenocconversion compared to pre-symptomatic mice. Data represent average log₂ fold change relative to pre-symptomatic, 4-month A β PP^{Swe}/PS1^{dE9} mice ($n = 3$ /condition). Statistics were one-way ANOVA comparing the abundances of each lipid species across normoxic and hypoxic conditions followed by Holm–Sidak *post hoc*

tests. $*p < 0.05$ for both impaired conditions relative to pre-symptomatic 4-month-old normoxic A β PP^{Swe}/PS1^{dE9} mice. The only other statistically significant change detected was an increase in LPC(21:0/0:0) in older symptomatic but not younger hypoxic A β PP^{Swe}/PS1^{dE9} mice ($\#p < 0.05$). (d) Comparison of pmol abundances of the six indicators of glycerophosphocholine metabolic impairment in pre-symptomatic 4-month normoxic A β PP^{Swe}/PS1^{dE9} mice ($n = 3$) and at symptomatic onset in 6–9-month normoxic A β PP^{Swe}/PS1^{dE9} mice ($n = 5$) or 4-month hypoxic A β PP^{Swe}/PS1^{dE9} mice ($n = 3$). Data represent mean species abundance (pmol per mg tissue wet weight) \pm SEM. Statistics were one-way ANOVAS (LPC(16:0/0:0): $F_{(2,8)} = 9.29$, $p = 0.008$; LPC(18:0/0:0): $F_{(2,8)} = 8.98$, $p = 0.009$, LPC(24:6/0:0): $F_{(2,8)} = 0.034$, LPC(25:6/0:0): $F_{(2,8)} = 6.42$, $p = 0.02$; LPC(O-18:0/0:0): $F_{(2,8)} = 7.81$, $p = 0.013$; and PC(O-22:6/2:0): $F_{(2,8)} = 10.35$, $p = 0.008$) with Holm–Sidak *post hoc* tests for multiple comparisons ($**p < 0.01$, $*p < 0.05$). All abundances for each comparison and statistics are reported in Supplemental Table S1. A β PP, amyloid precursor protein; Lyso-phosphatidylcholines; LPC(O), monoalkylglycerophosphocholine; PC(O), 1-alkyl,2-acylglycerophosphocholine.

(Non-Tg) littermates (Fig. 6d). Remodeling of LPC (O-18:1/0:0) to PC(O-18:1/2:0) increased significantly between 6 to 8 months in symptomatic Tg mice but not in age-matched Non-Tg littermates (Fig. 6d).

We quantified cPLA₂ α activity directly in temporal/parietal/entorhinal cortex over time (Fig. 6e). There was no change in cPLA₂ α activity in Non-Tg mice between 2 and 8 months of age (Fig. 6e). By contrast, cPLA₂ α activity decreased significantly in Tg mice at symptomatic onset (4-months of age) and increased significantly in fully impaired 6- and 8-month-old mice (Fig. 6e). To provide mechanistic insight into why PC(O)-PAF levels accumulated in symptomatic Tg mice, we examined PFAH1b subunit expression (Fig. 6f). The PFAH1b trimer is composed of two catalytic subunits, α_1 and/ or α_2 , and one regulatory subunit, LIS1 and is expressed by neurons not glia in brain (Escamez *et al.* 2012). α_2 and LIS1 protein levels did not change with age in Tg and Non-Tg littermates (Fig. 6f). PFAH1b α_1 protein expression significantly increased with age in both Tg and Non-Tg mice (Fig. 6f, Supplemental Figure S4). Because PFAH α_2/α_2 homodimers have a higher affinity for PC(O)-PAF than α_1/α_2 heterodimers or α_1/α_1 homodimers (Manya *et al.* 1999; Bonin *et al.* 2004), this shift in catalytic subunit expression is consistent with the accumulation of PC(O-18:1/2:0) over time in fully impaired Tg mice.

Discussion

In this study, we identify sequential changes in Land's cycle glycerophosphocholine metabolism that discriminate between pre-symptomatic, symptomatic, and fully impaired human A β PP mice. We used two different mouse models to ensure changes were indicative of behavioral indices of learning and memory impairment regardless of how or when pathological A β -deposition is induced and accumulates. Using an unbiased

lipidomic approach and direct biochemical assessments, we show that the glycerophosphocholine metabolomes of pre-symptomatic A β PP^{Swe}/PS1^{dE9} and N5 TgCRND8 mice are indistinguishable from littermate controls lacking human mutant A β PP. Upon symptomatic onset, cPLA₂ α activity is suppressed and LPC and LPC(O) levels are reduced in both the frontal and temporal/parietal/entorhinal cortices but not hippocampus of A β PP^{Swe}/PS1^{dE9} and N5 TgCRND8 mice. Critical metabolic indicators are decreases in abundance of LPC(16:0/0:0), LPC(18:0/0:0), LPC(24:6/0:0), LPC(25:6/0:0), LPC(O-18:0/0:0), and PC(O-22:6/2:0). When human A β PP animals become fully impaired, cPLA₂ α activity progressively increases. LPC and LPC(O) levels rise. The product to precursor ratio of PC(O-18:1/2:0) to PC(O-18:1/0:0) is progressively elevated indicative of the accumulation of this pro-inflammatory PC(O)-PAF. These changes are accompanied by an age-dependent shift in the expression of the PFAH1b catalytic subunits favoring α_1/α_2 and α_1/α_1 dimerization predicted to further reduce hydrolysis of PC(O)-PAF back to LPC(O) thus promoting accumulation of specific PAFs in Tg cortices.

This study helps to reconcile controversy as to whether PLA₂ activation or inhibition in AD is pathological. Our data indicate that cortical glycerophosphocholine remodeling is suppressed when pre-symptomatic A β PP mice transition to a symptomatic state. This suppression is the result of decreased cPLA₂ activity. Interestingly, we observed a specificity to this metabolism wherein some LPC and LPC(O) species that differ by only two carbons are not affected to the same extent as others. Group IV cPLA₂ α , assayed directly in this study, is known to preferentially hydrolyze glycerophosphocholines with arachidonic acid at the *sn*-2 position (Kita *et al.* 2006). Thus, the species-specific differences in metabolism detected here may reflect the enrichment of arachidonic acid in different subsets of precursors. In this study, we did not assay

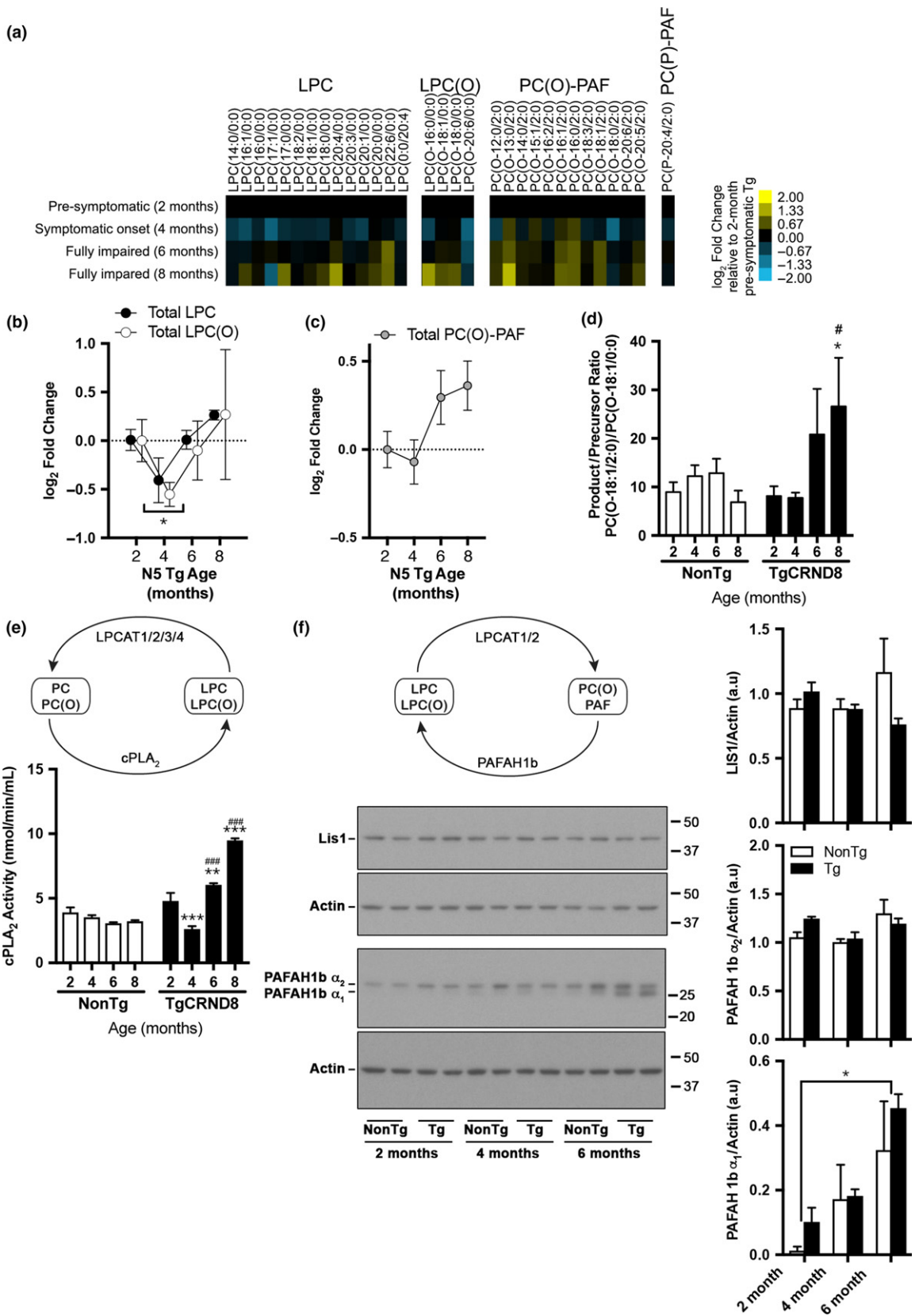


Fig. 6 Decreases and increases in Lands' cycle metabolism differentiate symptomatic onset from symptomatic progression in cortex of N5 TgCRND8 mice. (a) Heat map depicting changes in the glycerophosphocholine metabolic landscape of 2-month (pre-symptomatic, $n = 4$), 4-month (symptomatic onset, $n = 4$), 6-month (fully impaired, $n = 4$) and 8-month (fully impaired, $n = 3$) N5 TgCRND8 mice. Data represent \log_2 fold change relative to 2-month pre-symptomatic Tg mice. (b) Total LPC and LPC(O) levels decrease in 4-month-old mice when Tg mice become symptomatic; total LPC and LPC(O) levels are restored in fully impaired 6- and 8-month-old animals. Data represents mean \log_2 fold change \pm SEM relative to 2-month pre-symptomatic Tg mice. Statistics were 2-way ANOVA, main effect of age ($F_{(3,19)} = 4.1$, $p = 0.02$) $*p < 0.05$ relative to 2-month N5 Tg mice with Holm–Sidak *post hoc* tests for multiple comparisons. (c) Elevations in total PC(O)-PAF levels in fully impaired 6- and 8-month-old animals were not statistically significant. Data represents mean \log_2 fold change \pm SEM relative to 2-month N5 Tg mice. Statistics were a one-way ANOVA ($F_{(3,9)} = 2.26$, $p = 0.15$). (d) Product/Precursor ratios of PC(O-18:1/2:0)/PC(O-18:0/0:0) were performed to assess rate of LPC(O) to PC(O)-PAF remodeling. An increase in remodeling was detected between 6- and 8-month-old in Tg but not Non-Tg mice. Statistics were two-way ANOVA with a significant interaction ($F_{(3,25)} = 3.28$, $p = 0.037$), $*p < 0.05$ relative to 2-month pre-symptomatic Tg mice and $\#p < 0.05$ relative to age-matched Non-Tg mice with

Holm–Sidak *post hoc* tests for multiple comparisons. (e) Increases and decreases in cPLA₂ α activity distinguished symptomatic onset (4-month Tg) from fully impaired (6- and 8-month-old) mice. No age-dependent change in cPLA₂ α activity was observed in Non-Tg mice. Data represent mean \pm SEM nmol/min/mL of cPLA₂ activity. Statistics were two-way ANOVA with significant main effects of genotype and a significant interaction ($F_{(1,16)} = 125.7$, $p < 0.001$; $F_{(3,16)} = 56.2$, $p < 0.001$), $**p < 0.01$, $***p < 0.001$ relative to 2-month pre-symptomatic Tg mice and $\#\#\#p < 0.001$ relative to age-matched Non-Tg mice with Holm–Sidak *post hoc* tests for multiple comparisons. (f) PAFAH1b α_1 but not LIS1 or α_2 protein levels increase with age. Data represent western blots (left panel) and densitometry (right panel) of PAFAH protein subunit levels in 2-, 4-, and 6-month-old Non-Tg and Tg mice. Mean ratio to the actin loading control \pm SEM of each subunit are presented. Statistics were two-way ANOVA for each subunit. A significant main effect of age was detected: ($F_{(2,6)} = 8.78$, $p = 0.016$, $n = 2$ /ages/genotypes) with Holm–Sidak *post hoc* tests for multiple comparisons $*p < 0.05$ relative to 2-month-old mice. Longer exposures are provided in Supplemental Figure S4. Blots were probed simultaneously for α_1 and α_2 . Blots probed individually are also presented in Supplemental Figure S4. LPC, Lyso-phosphatidylcholines; LPC(O), monoalkylglycerophosphocholine; PAF, platelet-activating factor; PAFAH, acetylhydrolase; PC(O), 1-alkyl-2-acylglycerophosphocholine.

other PLA₂ isoforms but our findings are consistent with evidence that lower platelet iPLA₂ activity predicts risk of conversion from mild cognitive impairment to AD (Gattaz *et al.* 2014), while lower cortical total PLA₂ activity correlates with earlier AD onset (Gattaz *et al.* 1996; Ross *et al.* 1998). Elucidating substrate preference in future studies will enable a more precise targeting of the metabolic disruptions that precede phenoconversion. We also found that in fully impaired animals, cPLA₂ α activity rises and LPC levels are elevated. Likewise, levels of arachidonic acid and its metabolites increase in both CSF and brain of mid and late-stage AD patients (Montine *et al.* 1999) as arachidonic acid is preferentially hydrolyzed from glycerophosphocholines by cPLA₂ α (Diez *et al.* 1992). The rise in LPC levels detected here is also consistent with the increase in glycerophosphocholine metabolite levels in postmortem AD brain correlating with severity of cognitive decline and psychosis (Sweet *et al.* 2002). In concert with these increases, we found that downstream PC(O)-PAF metabolites accumulate in N5 TgCRND8 mice. This accumulation has been seen in network analyses of metabolic changes associated with AD progression in humans (Toledo *et al.* 2017), wherein higher levels of circulating PC(O) lipids correlate with a faster rate of AD cognitive decline (Toledo *et al.* 2017). Likewise, PC(O)-PAF levels are elevated in the entorhinal cortex of late-stage AD patients' post-mortem (Ryan *et al.* 2009). Taken together, these data provide converging evidence to indicate that the onset and progression of AD are distinguished by distinct changes in Land's cycle metabolism of glycerophosphocholines. Transient cPLA₂ α suppression and

reductions in *lyso*-metabolites in cortex associates with symptomatic onset, while increased cPLA₂ α activity and accumulation of PC(O)-PAFs associate with disease progression.

The biphasic changes observed in cPLA₂ α activity in this study were both age-independent and required pre-existing A β pathology. Both A β PP^{Swe}/PS1^{dE9} and N5 TgCRND8 mice exhibited the same decreases in Land's cycle remodeling despite their age differential at symptomatic onset. A β PP^{Swe}/PS1^{dE9} mice first exhibit behavioral impairment between 6 and 9 months of age (Garcia-Alloza *et al.* 2006; Reiserer *et al.* 2007; Yang *et al.* 2015). TgCRND8 mice are symptomatic at 4 months of age (Chishti *et al.* 2001; Granger *et al.* 2016). Moreover, levels of the same critical indicators of cPLA₂ α suppression, LPC(16:0/0:0), LPC(18:0/0:0), LPC(24:6/0:0), LPC(25:6/0:0), and LPC(O-18:0/0:0), decline in younger A β PP^{Swe}/PS1^{dE9} mice when symptomatic onset is accelerated by hypoxic insult. Chronic intermittent hypoxia is an environmental risk factor that results in earlier manifestation of learning and memory deficits, enhanced A β biogenesis, and exacerbated tau pathologies in human A β PP mouse models (Sun *et al.* 2006; Li *et al.* 2009; Gao *et al.* 2013; Zhang *et al.* 2013; Liu *et al.* 2016). This same insult is associated with a higher incidence of AD phenoconversion in humans (Daulatzai 2013). Interestingly, we show here that decreased glycerophosphocholine metabolite abundances following hypoxic insult depends on pre-existing A β pathology. WT littermates subjected to the same chronic hypoxic insult did not show the same degree of lipidomic disruption as A β PP^{Swe}/PS1^{dE9} mice. Together, these data indicate that hypoxia alone does not alter enzymatic activity

to the same extent in the absence of A β pathology. Moreover, we did not detect any age-associated changes in cortical cPLA $_2\alpha$ activity in normoxic mice devoid of human A β PP between 2 and 8 months of age. These data provide converging evidence to indicate that suppression of cPLA $_2\alpha$ activity is an indicator of experimental phenoconversion and that hypoxic risk of critical metabolic defects associated with cognitive decline is likely enhanced in preclinical AD patients.

Age, however, remains the primary risk factor for AD (Fjell *et al.* 2014). Disease incidence increases dramatically after 60 years of age (Kawas *et al.* 2000). Herrup (2010) has proposed a model in which normal aging, vascular trauma, and chronic neuroinflammation renders the elderly brain vulnerable to the amyloid cascade. Here, any injury that triggers a chronic neuroinflammatory response can precipitate a metabolic ‘change in state’. This ‘change of state’ is envisioned as a convergence of critical metabolic dysfunctions that exacerbate the amyloid cascade and precipitates cognitive decline (Herrup 2010). We found here that while biphasic changes in cPLA $_2\alpha$ activity are likely age-independent, these changes are also accompanied by an age-dependent shift in the relative expression of the catalytic α_1 and α_2 subunits of PAFAH1b in both TgCNRD8 and Non-Tg littermates. The PAFAH1b trimer is composed two catalytic subunits, α_1 and/ or α_2 and one regulatory subunit, LIS1. PAFAH1b α_2 homodimers more effectively hydrolyze PC(O)-PAF to LPC(O) than PAFAH1b α_2/α_1 heterodimers or α_1/α_1 homodimers (Manya *et al.* 1999; Bonin *et al.* 2004). Thus, any shift in protein expression favoring complexes composed of α_2/α_1 and α_1/α_1 is predicted to reduce PC(O)-PAF hydrolysis and promote PC(O)-PAF accumulation. Our data indicate that younger adult mice predominantly express PAFAH1b α_2 , while older mice increasingly express PAFAH1b α_1 at the protein level. These experimental data are supported by evidence that metabolism of PC(O)-PAFs is disrupted in AD (Ryan *et al.* 2009; de Leeuw *et al.* 2017) with A β_{42} promoting remodeling of LPC(O) to PC(O)-PAF (Ryan *et al.* 2009; Simmons *et al.* 2014; McHale-Owen and Bate 2018). Elevated cortical PC(O)-PAF levels have been linked mechanistically to the progression of other neuroinflammatory-associated dementias (Gelbard *et al.* 1994; Kelesidis *et al.* 2015). Thus, age-dependent reduction in PC(O)-PAF hydrolysis likely represents another metabolic correlate of cognitive decline over the course of AD.

In summary, we identify in this study two defining disruptions in Land’s cycle glycerophosphocholine metabolism that distinguish pre-symptomatic, from symptomatic, from fully impaired human A β PP mice. These data provide the first direct evidence that the cortical glycerophosphocholine metabolome is differentially regulated at symptomatic onset and over the course of symptomatic decline in two mouse models of AD.

Acknowledgments and conflict of interest disclosure

MWG and SPMS received Ontario Graduate Scholarships; APB received an Alzheimer Society of Canada studentship; MT received a Natural Science Research Council studentship. This study was funded by a University of Ottawa and Shanghai Jiao Tong University Joint Medical Research Program grant to WL and SALB, Canadian Institute of Health Research (MOP#311838) and Natural Science Research Council operating grant (#5377) to SALB, and Chinese National Sciences Foundation (No. 81370470, No. 81430021), National Basic Research Program (No. 2011CB510003 and No. 81771521), and Collaborative Innovation Center for Brain Science to WL. We thank Louis Dacquay for confirmatory data analysis replicating these analyses performed as part of his participation in our graduate class BCH8110 (University of Ottawa). The authors have no conflict of interest to report.

All experiments were conducted in compliance with the ARRIVE guidelines.

Open science badges

This article has received a badge for ***Open Materials*** because it provided all relevant information to reproduce the study in the manuscript. The complete Open Science Disclosure form for this article can be found at the end of the article. More information about the Open Practices badges can be found at <https://cos.io/our-services/open-science-badges/>.

Supporting information

Additional supporting information may be found online in the Supporting Information section at the end of the article.

Figure S1. Land’s cycle metabolism of glycerophosphocholines.

Figure S2. Verification that sphingomyelins are not detected in our glycerophosphocholine metabolite and second messenger LC-ESI-MS/MS profiles.

Figure S3. Analysis of critical glycerophospholipidome metabolites in 4-month-old hypoxic compared to normoxic WT mice.

Figure S4. Western analysis of PAFAH α_2 and α_1 catalytic subunits.

Table S1. Mean pmol comparisons of frontal cortex glycerophosphocholine metabolites and signaling molecules in WT and AbPP/PS1 mice.

References

- Bateman R. J., Xiong C., Benzinger T. L. *et al.* (2012) Clinical and biomarker changes in dominantly inherited Alzheimer’s disease. *N. Engl. J. Med.* **367**, 795–804.
- Benjamini Y., Kreiger A. and Yekutieli D. (2006) Adaptive linear step-up procedures that control the false discovery rate. *Biometrika* **93**, 491–507.
- Bennett S. A. L., Valenzuela N., Xu H., Franko B., Fai S. and Figeys D. (2013) Using neurolipidomics to identify phospholipid mediators

- of synaptic (dys)function in Alzheimer's disease. *Front. Physiol.* **4**, 168.
- Bierer L. M., Hof P. R., Purohit D. P., Carlin L., Schmeidler J., Davis K. L. and Perl D. P. (1995) Neocortical neurofibrillary tangles correlate with dementia severity in Alzheimer's disease. *Arch. Neurol.* **52**, 81–88.
- Blanchard A. P., McDowell G. S., Valenzuela N. *et al.* (2013) Visualization and phospholipid identification (VaLID): online integrated search engine capable of identifying and visualizing glycerophospholipids with given mass. *Bioinformatics* **29**, 284–285.
- Bligh E. C. and Dyer W. J. (1959) A rapid method of lipid extraction and purification. *Can. J. Biochem.* **37**, 911–917.
- Bonin F., Ryan S. D., Migahed L., Mo F., Lallier J., Franks D. J., Arai H. and Bennett S. A. L. (2004) Anti-apoptotic actions of the platelet activating factor acetylhydrolase 1 alpha 2 catalytic subunit. *J. Biol. Chem.* **279**, 52425–52436.
- Buchhave P., Minthon L., Zetterberg H., Wallin A. K., Blennow K. and Hansson O. (2012) Cerebrospinal fluid levels of beta-amyloid 1-42, but not of tau, are fully changed already 5 to 10 years before the onset of Alzheimer dementia. *Arch. Gen. Psychiatry* **69**, 98–106.
- Burke J. E. and Dennis E. A. (2009) Phospholipase A2 biochemistry. *Cardiovasc. Drugs Ther.* **23**, 49–59.
- Chalbot S., Zetterberg H., Blennow K., Fladby T., Grundke-Iqbal I. and Iqbal K. (2009) Cerebrospinal fluid secretory Ca²⁺-dependent phospholipase A2 activity is increased in Alzheimer disease. *Clin. Chem.* **55**, 2171–2179.
- Chang B., Hawes N. L., Hurd R. E., Davisson M. T., Nusinowitz S. and Heckenlively J. R. (2002) Retinal degeneration mutants in the mouse. *Vision. Res.* **42**, 517–525.
- Chishti M. A., Yang D. S., Janus C. *et al.* (2001) Early-onset amyloid deposition and cognitive deficits in transgenic mice expressing a double mutant form of amyloid precursor protein 695. *J. Biol. Chem.* **276**, 21562–21570.
- Daulatzai M. A. (2013) Death by a thousand cuts in Alzheimer's disease: hypoxia—the prodrome. *Neurotox. Res.* **24**, 216–243.
- Diez E., Louis-Flamberg P., Hall R. H. and Mayer R. J. (1992) Substrate specificities and properties of human phospholipases A2 in a mixed vesicle model. *J. Biol. Chem.* **267**, 18342–18348.
- Doody R. S., Demirovic J., Ballantyne C. M., Chan W., Barber R., Powell S. and Pavlik V. (2015) Lipoprotein-associated phospholipase A2, homocysteine, and Alzheimer's disease. *Alzheimers Dement. (Amst)* **1**, 464–471.
- Dubois B., Hampel H., Feldman H. H. *et al.* (2016) Preclinical Alzheimer's disease: definition, natural history, and diagnostic criteria. *Alzheimers Dement.* **12**, 292–323.
- Escamez T., Bahamonde O., Tabares-Seisdedos R., Vieta E., Martinez S. and Echevarria D. (2012) Developmental dynamics of PAFAH1B subunits during mouse brain development. *J. Comp. Neurol.* **520**, 3877–3894.
- Fagan A. M., Xiong C., Jasielc M. S. *et al.* (2014) Longitudinal change in CSF biomarkers in autosomal-dominant Alzheimer's disease. *Sci. Transl. Med.* **6**, 226ra230.
- Fahy E., Cotter D., Sud M. and Subramaniam S. (2011) Lipid classification, structures and tools. *Biochim. Biophys. Acta* **1811**, 637–647.
- Farooqui A. A. and Horrocks L. A. (2006) Phospholipase A2-generated lipid mediators in the brain: the good, the bad, and the ugly. *Neuroscientist* **12**, 245–260.
- Faul F., Erdfelder E., Lang A. G. and Buchner A. (2007) G*Power 3: a flexible statistical power analysis program for the social, behavioral, and biomedical sciences. *Behav. Res. Methods* **39**, 175–191.
- Fjell A. M., McEvoy L., Holland D., Dale A. M., Walhovd K. B. and Alzheimer's Disease Neuroimaging I. (2014) What is normal in normal aging? Effects of aging, amyloid and Alzheimer's disease on the cerebral cortex and the hippocampus. *Prog. Neurobiol.* **117**, 20–40.
- Gao L., Tian S., Gao H. and Xu Y. (2013) Hypoxia increases Abeta-induced tau phosphorylation by calpain and promotes behavioral consequences in AD transgenic mice. *J. Mol. Neurosci.* **51**, 138–147.
- Garcia-Alloza M., Robbins E. M., Zhang-Nunes S. X. *et al.* (2006) Characterization of amyloid deposition in the APP^{swe}/PS1^{dE9} mouse model of Alzheimer disease. *Neurobiol. Dis.* **24**, 516–524.
- Gattaz W. F., Cairns N. J., Levy R., Forstl H., Braus D. F. and Maras A. (1996) Decreased phospholipase A2 activity in the brain and in platelets of patients with Alzheimer's disease. *Eur. Arch. Psychiatry Clin. Neurosci.* **246**, 129–131.
- Gattaz W. F., Forlenza O. V., Talib L. L., Barbosa N. R. and Bottino C. M. (2004) Platelet phospholipase A(2) activity in Alzheimer's disease and mild cognitive impairment. *J. Neural. Transm.* **111**, 591–601.
- Gattaz W. F., Talib L. L., Schaeffer E. L., Diniz B. S. and Forlenza O. V. (2014) Low platelet iPLA(2) activity predicts conversion from mild cognitive impairment to Alzheimer's disease: a 4-year follow-up study. *J. Neural. Transm.* **121**, 193–200.
- Gelbard H. A., Nottet H. S. L. M., Swindells S. *et al.* (1994) Platelet-activating factor: a candidate human immunodeficiency virus type 1-induced neurotoxin. *J. Virol.* **68**, 4628–4635.
- Granger M. W., Franko B., Taylor M. W., Messier C., George-Hyslop P. S. and Bennett S. A. L. (2016) A TgCRND8 mouse model of Alzheimer's disease exhibits sexual dimorphisms in behavioral indices of cognitive reserve. *J. Alzheimers Dis.* **51**, 757–773.
- Haass C. and Selkoe D. J. (2007) Soluble protein oligomers in neurodegeneration: lessons from the Alzheimer's amyloid beta-peptide. *Nat. Rev. Mol. Cell Biol.* **8**, 101–112.
- Herrup K. (2010) Reimagining Alzheimer's disease—an age-based hypothesis. *J. Neurosci.* **30**, 16755–16762.
- de Hoon M. J., Imoto S., Nolan J. and Miyano S. (2004) Open source clustering software. *Bioinformatics* **20**, 1453–1454.
- Kawas C., Gray S., Brookmeyer R., Fozard J. and Zonderman A. (2000) Age-specific incidence rates of Alzheimer's disease: the Baltimore Longitudinal Study of Aging. *Neurology* **54**, 2072–2077.
- Kelesidis T., Papanikolaou V., Detopoulou P., Fragopoulou E., Chini M., Lazanas M. C. and Antonopoulou S. (2015) The role of platelet-activating factor in chronic inflammation, immune activation, and comorbidities associated with HIV infection. *AIDS Rev.* **17**, 191–201.
- Kita Y., Ohto T., Uozumi N. and Shimizu T. (2006) Biochemical properties and pathophysiological roles of cytosolic phospholipase A2s. *Biochim. Biophys. Acta* **1761**, 1317–1322.
- de Leeuw F. A., Peeters C. F. W., Kester M. I. *et al.* (2017) Blood-based metabolic signatures in Alzheimer's disease. *Alzheimers Dement. (Amst)* **8**, 196–207.
- Li L., Zhang X., Yang D., Luo G., Chen S. and Le W. (2009) Hypoxia increases Abeta generation by altering beta- and gamma-cleavage of APP. *Neurobiol. Aging* **30**, 1091–1098.
- Liu H., Qiu H., Yang J., Ni J. and Le W. (2016) Chronic hypoxia facilitates Alzheimer's disease through demethylation of gamma-secretase by downregulating DNA methyltransferase 3b. *Alzheimers Dement.* **12**, 130–143.
- Manya H., Aoki J., Kato H., Ishii J., Hino S., Arai H. and Inoue K. (1999) Biochemical characterization of various catalytic complexes of the brain platelet-activating factor acetylhydrolase. *J. Biol. Chem.* **274**, 31827–31832.
- Mapstone M., Cheema A. K., Fiandaca M. S. *et al.* (2014) Plasma phospholipids identify antecedent memory impairment in older adults. *Nat. Med.* **20**, 415–418.

- McHale-Owen H. and Bate C. (2018) Cholesterol ester hydrolase inhibitors reduce the production of synaptotoxic amyloid-beta oligomers. *Biochim. Biophys. Acta* **1864**, 649–659.
- Montine T. J., Markesbery W. R., Zackert W., Sanchez S. C., Roberts L. J., 2nd and Morrow J. D. (1999) The magnitude of brain lipid peroxidation correlates with the extent of degeneration but not with density of neuritic plaques or neurofibrillary tangles or with APOE genotype in Alzheimer's disease patients. *Am. J. Pathol.* **155**, 863–868.
- Mulder C., Wahlund L. O., Teerlink T., Blomberg M., Veerhuis R., van Kamp G. J., Scheltens P. and Scheffer P. G. (2003) Decreased lysophosphatidylcholine/phosphatidylcholine ratio in cerebrospinal fluid in Alzheimer's disease. *J. Neural. Transm.* **110**, 949–955.
- Prescott S. M., Zimmerman G. A., Stafforini D. M. and McIntyre T. M. (2000) Platelet activating factor and related lipid mediators. *Annu. Rev. Biochem.* **69**, 419–445.
- Proitsi P., Kim M., Whaley L. *et al.* (2017) Association of blood lipids with Alzheimer's disease: a comprehensive lipidomics analysis. *Alzheimers Dement.* **13**, 140–151.
- Reiserer R. S., Harrison F. E., Syverud D. C. and McDonald M. P. (2007) Impaired spatial learning in the APPSwe + PSEN1DeltaE9 bigenic mouse model of Alzheimer's disease. *Genes Brain Behav.* **6**, 54–65.
- Ross B. M., Moszczynska A., Erlich J. and Kish S. J. (1998) Phospholipid-metabolizing enzymes in Alzheimer's disease: increased lysophospholipid acyltransferase activity and decreased phospholipase A2 activity. *J. Neurochem.* **70**, 786–793.
- Ryan S. D., Whitehead S. N., Swayne L. A. *et al.* (2009) Amyloid- β 42 signals tau hyperphosphorylation and compromises neuronal viability by disrupting alkylacylglycerophosphocholine metabolism. *Proc. Natl Acad. Sci. USA* **106**, 20936–20941.
- Saldanha A. J. (2004) Java Treeview—extensible visualization of microarray data. *Bioinformatics* **20**, 3246–3248.
- Shindou H. and Shimizu T. (2009) Acyl-CoA: lysophospholipid acyltransferases. *J. Biol. Chem.* **284**, 1–5.
- Simmons C., Ingham V., Williams A. and Bate C. (2014) Platelet-activating factor antagonists enhance intracellular degradation of amyloid-beta42 in neurons via regulation of cholesterol ester hydrolases. *Alzheimers Res. Ther.* **6**, 15.
- Smesny S., Stein S., Willhardt I., Lasch J. and Sauer H. (2008) Decreased phospholipase A2 activity in cerebrospinal fluid of patients with dementia. *J. Neural. Transm.* **115**, 1173–1179.
- Sud M., Fahy E., Cotter D. *et al.* (2007) LMSD: LIPID MAPS structure database. *Nucleic Acids Res.* **35**, D527–D532.
- Sun X., He G., Qing H., Zhou W., Dobie F., Cai F., Staufenbiel M., Huang L. E. and Song W. (2006) Hypoxia facilitates Alzheimer's disease pathogenesis by up-regulating BACE1 gene expression. *Proc. Natl Acad. Sci. USA* **103**, 18727–18732.
- Sweet R. A., Panchalingam K., Pettegrew J. W., McClure R. J., Hamilton R. L., Lopez O. L., Kaufer D. I., DeKosky S. T. and Klunk W. E. (2002) Psychosis in Alzheimer disease: postmortem magnetic resonance spectroscopy evidence of excess neuronal and membrane phospholipid pathology. *Neurobiol. Aging* **23**, 547–553.
- Toledo J. B., Arnold M., Kastenmuller G. *et al.* (2017) Metabolic network failures in Alzheimer's disease—A biochemical road map. *Alzheimers Dement.* **13**, 965–984.
- Toye A. A., Lippiat J. D., Proks P. *et al.* (2005) A genetic and physiological study of impaired glucose homeostasis control in C57BL/6J mice. *Diabetologia* **48**, 675–686.
- Wang F., Blanchard A. P., Elisma F., Granger M., Xu H., Bennett S. A. L., Figeys D. and Zou H. (2013) Phosphoproteome analysis of an early onset mouse model (TgCRND8) of Alzheimer's disease reveals temporal changes in neuronal and glia signaling pathways. *Proteomics* **13**, 1292–1305.
- Xia J., Sinelnikov I. V., Han B. and Wishart D. S. (2015) MetaboAnalyst 3.0—making metabolomics more meaningful. *Nucleic Acids Res.* **43**, W251–W257.
- Xu H., Valenzuela N., Fai S., Figeys D. and Bennett S. A. L. (2013) Targeted lipidomics - advances in profiling lysophosphocholine and platelet-activating factor second messengers. *FEBS J.* **280**, 5652–5667.
- Yang R. Y., Zhao G., Wang D. M. *et al.* (2015) DL0410 can reverse cognitive impairment, synaptic loss and reduce plaque load in APP/PS1 transgenic mice. *Pharmacol. Biochem. Behav.* **139**, 15–26.
- Zhang X., Li L., Zhang X. *et al.* (2013) Prenatal hypoxia may aggravate the cognitive impairment and Alzheimer's disease neuropathology in APPSwe/PS1A246E transgenic mice. *Neurobiol. Aging* **34**, 663–678.

Supplementary Data

Distinct disruptions in Land's cycle remodeling of glycerophosphocholines in murine cortex mark symptomatic onset and progression in two Alzheimer's Disease mouse models

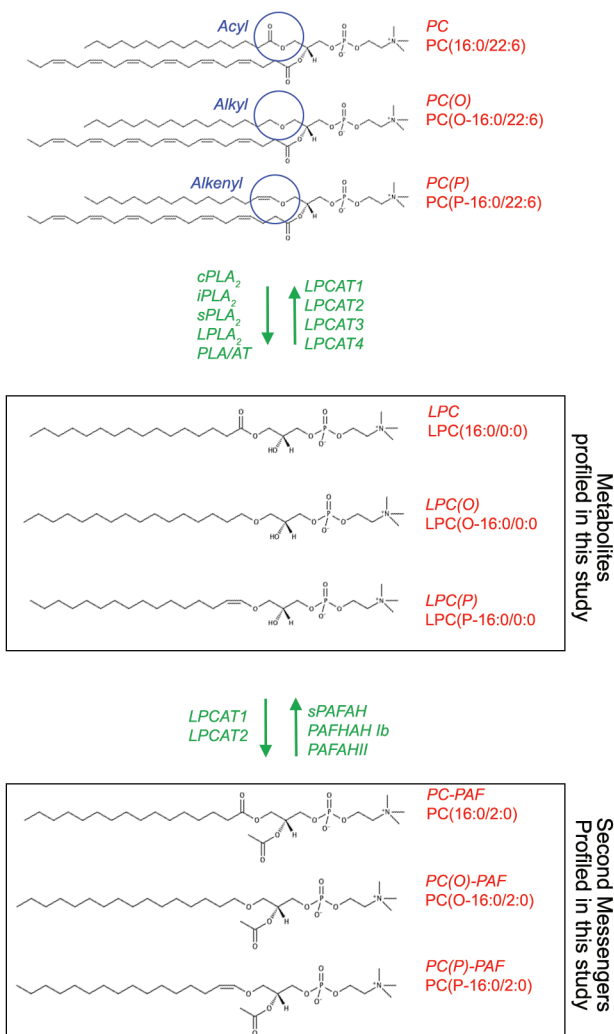
Matthew W. Granger^a, Hui Liu^{b†}, Caitlin F. Fowler^a, Alexandre P. Blanchard^a, Matthew Taylor^a, Samantha P.M. Sherman^a, Hongbin Xu^{a*}, Weidong Le^{b*}, Steffany A.L. Bennett^{a*}

^aNeural Regeneration Laboratory, Ottawa Institute of Systems Biology, University of Ottawa Brain and Mind Research Institute, Centre for Catalysis Research and Innovation, Department of Biochemistry, Microbiology, and Immunology, University of Ottawa, Ottawa, ON, Canada,

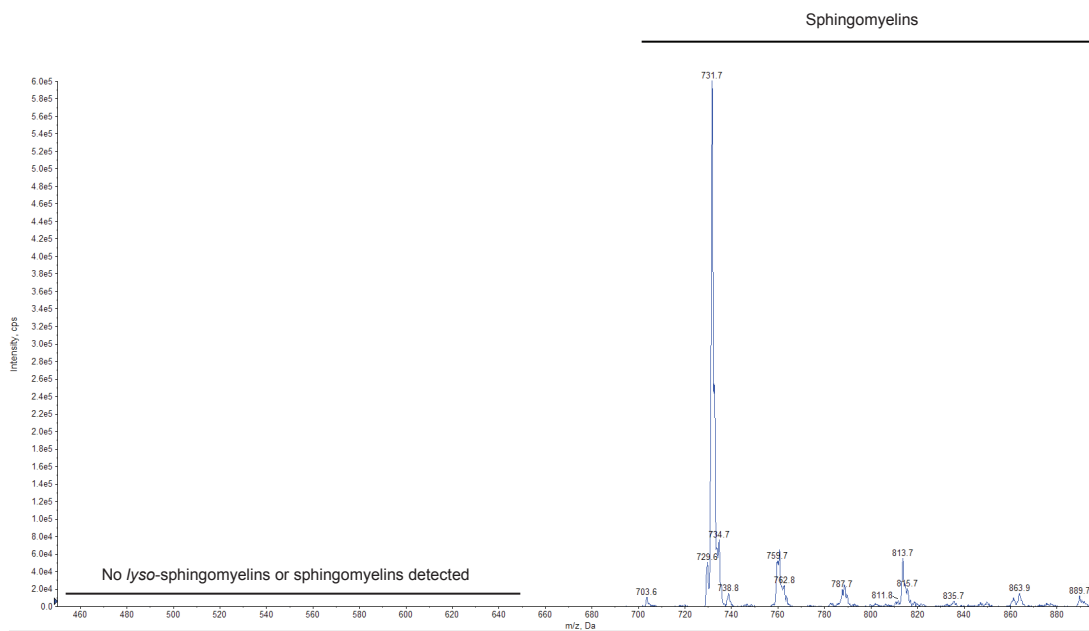
^bInstitute of Neurology, Ruijin Hospital, Shanghai Jiao Tong University School of Medicine, Shanghai, PR China.

SUPPLEMENTAL TABLE 1: Mean pmol comparisons of frontal cortex glycerophosphocholine metabolites and signaling molecules in WT and AβPP/PS1 mice

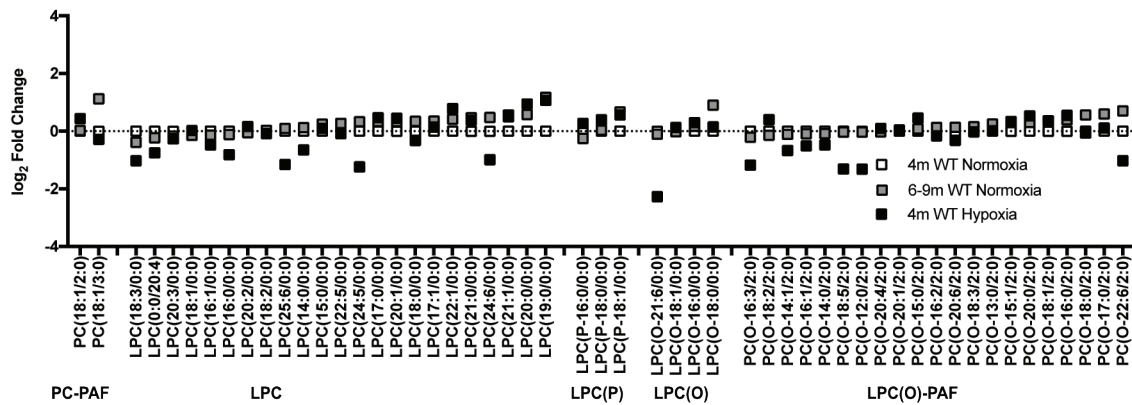
Subclass	Species	WT						AβPP/PS1						WT (4 months) vs AβPP/PS1 (4 months)			
		Normoxia		6-9 months		Hypoxia 4 months		ANOVA p-value	Normoxia		6-9 months		Hypoxia 4 months		ANOVA p-value	T ratio	q Value
		4 months	SEM	Mean	SEM	Mean	SEM		Mean	SEM	Mean	SEM	Mean	SEM			
PC-PAF	PC(18:1/3:0)	0.0056	0.0022	0.0124	0.0044	0.0036	0.0003	0.3430	0.0073	0.0020	0.0060	0.0012	0.0043	0.0015	0.4904	0.5718	0.8516
	PC(18:1/2:0)	0.0146	0.0051	0.0147	0.0030	0.0210	0.0082	0.6714	0.0204	0.0046	0.0237	0.0022	0.0180	0.0039	0.4820	0.8445	0.8516
	Total	0.0203	0.0060	0.0218	0.0018	0.0234	0.0082	0.9547	0.0277	0.0045	0.0218	0.0018	0.0190	0.0057	0.3608	0.9867	0.8516
LPC	LPC(21:1/0:0)	0.0017	0.0003	0.0026	0.0005	0.0028	0.0013	0.6313	0.0028	0.0003	0.0037	0.0005	0.0036	0.0009	0.6313	2.5930	0.7777
	LPC(18:3/0:0)	0.0049	0.0022	0.0034	0.0006	0.0021	0.0005	0.3583	0.0043	0.0015	0.0027	0.0009	0.0023	0.0004	0.4121	0.2253	0.9471
	LPC(17:1/0:0)	0.0097	0.0018	0.0134	0.0031	0.0123	0.0050	0.7714	0.0141	0.0034	0.0129	0.0017	0.0120	0.0035	0.8848	1.1440	0.8516
	LPC(15:0/0:0)	0.0143	0.0032	0.0188	0.0057	0.0168	0.0064	0.8525	0.0209	0.0055	0.0173	0.0033	0.0176	0.0044	0.8195	1.0370	0.8516
	LPC(24:6/0:0)	0.0129	0.0052	0.0437	0.0321	0.0067	0.0027	0.5647	0.0324	0.0094	0.0105*	0.0027	0.0090*	0.0019	0.034*	1.8150	0.8516
	LPC(21:0/0:0)	0.0160	0.0034	0.0220	0.0029	0.0247	0.0120	0.6634	0.0163	0.0017	0.0355*	0.0040	0.0229	0.0060	0.0316*	0.0789	0.9574
	LPC(19:0/0:0)	0.0111	0.0027	0.0257	0.0048	0.0267	0.0121	0.2949	0.0175	0.0029	0.0322	0.0053	0.0345	0.0057	0.1311	1.6150	0.8516
	LPC(22:5/0:0)	0.0275	0.0062	0.0354	0.0079	0.0269	0.0067	0.9370	0.0271	0.0071	0.0309	0.0078	0.0310	0.0095	0.9370	0.0424	0.9682
	LPC(14:0/0:0)	0.0306	0.0083	0.0365	0.0103	0.0201	0.0072	0.5187	0.0320	0.0098	0.0285	0.0091	0.0245	0.0055	0.8707	0.0934	0.9574
	LPC(20:3/0:0)	0.0371	0.0091	0.0342	0.0075	0.0330	0.0103	0.9534	0.0623	0.0155	0.0335	0.0033	0.0359	0.0104	1.0598	1.4020	0.8516
	LPC(20:2/0:0)	0.0474	0.0095	0.0479	0.0095	0.0575	0.0189	0.8338	0.0723	0.0120	0.0624	0.0116	0.0703	0.0188	0.8582	1.6270	0.8516
	LPC(24:5/0:0)	0.0746	0.0340	0.1188	0.0476	0.0312	0.0147	0.3798	0.0842	0.0352	0.0623	0.0160	0.0617	0.0064	0.5213	0.4005	0.8848
	LPC(22:1/0:0)	0.0523	0.0054	0.0725	0.0120	0.1046	0.0432	0.3555	0.0573	0.0145	0.1267	0.0133	0.1073	0.0311	0.0828	0.3231	0.8848
	LPC(17:0/0:0)	0.0679	0.0151	0.0923	0.0245	0.1114	0.0527	0.6957	0.1049	0.0125	0.1080	0.0215	0.1216	0.0299	0.8822	1.8880	0.8516
	LPC(18:2/0:0)	0.1358	0.0306	0.1461	0.0325	0.1352	0.0394	0.9666	0.2810	0.1560	0.1176	0.0241	0.1296	0.0299	0.3105	0.9134	0.8516
	LPC(20:0/0:0)	0.1020	0.0246	0.1497	0.0255	0.2293	0.1105	0.3743	0.1292	0.0239	0.2277	0.0409	0.2455	0.0640	0.2589	0.7930	0.8516
	LPC(16:1/0:0)	0.2152	0.0567	0.1969	0.0340	0.1565	0.0430	0.6764	0.1832	0.0351	0.1810	0.0468	0.1907	0.0362	0.9878	0.4799	0.8848
	LPC(25:6/0:0)	0.1883	0.1216	0.7429	0.6715	0.0813	0.0497	0.6530	0.3728	0.1316	0.0778*	0.0238	0.0815*	0.0181	0.0217*	1.0300	0.8516
	LPC(20:1/0:0)	0.2202	0.0288	0.2858	0.0402	0.3164	0.0866	0.5181	0.2746	0.0222	0.4021	0.0437	0.3817	0.0770	0.2469	1.4960	0.8516
	LPC(0:0/2:0)	3.7956	1.2575	3.2479	0.6256	2.1360	0.4377	0.4291	2.6946	0.5049	2.6902	0.5210	1.9483	0.1950	0.5326	0.8125	0.8516
LPC(18:1/0:0)	2.2538	0.5572	2.0934	0.4538	2.5393	0.9659	0.8809	3.0168	0.5163	3.1284	0.3720	2.8375	0.6681	0.9148	1.0040	0.8516	
LPC(18:0/0:0)	5.1649	1.0693	6.8183	1.4378	3.9312	0.1651	0.3122	7.3510	0.8612	5.0026*	0.4549	4.1094*	0.3880	0.009*	1.7390	0.8516	
LPC(16:0/0:0)	7.4005	1.7365	7.3644	1.9419	4.0159	0.4134	0.3957	9.1524	0.7865	5.1759*	0.8128	3.9594*	0.6742	0.0082*	0.9190	0.8516	
Total	16.0973	3.3961	18.3783	1.8803	11.8986	1.2156	0.1161	21.3268	0.8614	14.9082	1.0708	13.1685	2.8533	0.1095	1.4930	0.8516	
LPC(P)	LPC(P-18:1/0:0)	0.0049	0.0016	0.0073	0.0011	0.0089	0.0046	0.5835	0.0063	0.0010	0.0081	0.0009	0.0101	0.0024	0.2636	0.7420	0.8516
	LPC(P-16:0/0:0)	0.0148	0.0037	0.0136	0.0038	0.0204	0.0088	0.6558	0.0173	0.0019	0.0167	0.0026	0.0213	0.0052	0.6381	0.6011	0.8516
	LPC(P-18:0/0:0)	0.0740	0.0199	0.0780	0.0161	0.1011	0.0351	0.1605	0.0607	0.0039	0.1165	0.0201	0.1293	0.0322	0.1605	0.6559	0.8516
Total	0.0937	0.0251	0.0988	0.0088	0.1304	0.0485	0.7839	0.0844	0.0057	0.1380	0.0231	0.0802	0.0144	0.2290	0.3613	0.8848	
LPC(O)	LPC(O-21:6/0:0)	0.0059	0.0022	0.0177	0.0147	0.0012	0.0003	0.6074	0.0106	0.0079	0.0018	0.0005	0.0009	0.0003	0.2074	0.5731	0.8516
	LPC(O-18:1/0:0)	0.0080	0.0016	0.0085	0.0020	0.0098	0.0037	0.9053	0.0096	0.0008	0.0102	0.0026	0.0113	0.0030	0.9053	0.8944	0.8516
	LPC(O-16:0/0:0)	0.0119	0.0025	0.0152	0.0050	0.0155	0.0053	0.8326	0.0151	0.0014	0.0150	0.0031	0.0177	0.0046	0.8326	1.1170	0.8516
LPC(O-18:0/0:0)	0.0155	0.0031	0.0322	0.0076	0.0182	0.0057	0.2146	0.0389	0.0048	0.0185*	0.0029	0.0222*	0.0042	0.0132*	0.40950	0.4324	
Total	0.0412	0.0085	0.0736	0.0120	0.0445	0.0144	0.2818	0.0742	0.0092	0.0455	0.0085	0.0331	0.0064	0.0160*	2.6350	0.7777	
PC(O)-PAF	PC(O-17:0/2:0)	0.0023	0.0003	0.0036	0.0006	0.0026	0.0008	0.4012	0.0032	0.0002	0.0038	0.0010	0.0035	0.0009	0.9434	2.4960	0.7777
	PC(O-16:3/2:0)	0.0082	0.0021	0.0075	0.0019	0.0034	0.0005	0.2513	0.0051	0.0019	0.0056	0.0014	0.0046	0.0007	0.8796	1.0950	0.8516
	PC(O-13:0/2:0)	0.0112	0.0022	0.0132	0.0014	0.0117	0.0028	0.7441	0.0139	0.0045	0.0132	0.0035	0.0126	0.0035	0.9763	0.5390	0.8541
	PC(O-15:0/2:0)	0.0091	0.0012	0.0106	0.0025	0.0135	0.0039	0.5929	0.0149	0.0047	0.0150	0.0031	0.0142	0.0039	0.9899	1.1960	0.8516
	PC(O-15:1/2:0)	0.0133	0.0017	0.0170	0.0026	0.0175	0.0037	0.5952	0.0111	0.0035	0.0176	0.0042	0.0172	0.0047	0.5603	0.5654	0.8516
	PC(O-18:5/2:0)	0.0203	0.0086	0.0195	0.0047	0.0070	0.0008	0.2576	0.0142	0.0042	0.0182	0.0054	0.0090	0.0005	0.4562	0.6374	0.8516
	PC(O-20:1/2:0)	0.0182	0.0046	0.0187	0.0032	0.0182	0.0032	0.9927	0.0122	0.0041	0.0307	0.0113	0.0220	0.0062	0.4437	0.9737	0.8516
	PC(O-22:6/2:0)	0.0163	0.0064	0.0408	0.0232	0.0074	0.0015	0.4538	0.0326	0.0070	0.0104*	0.0020	0.0099*	0.0007	0.0081*	1.7190	0.8516
	PC(O-18:2/2:0)	0.0190	0.0026	0.0185	0.0040	0.0291	0.0097	0.4007	0.0240	0.0074	0.0284	0.0086	0.0309	0.0101	0.8891	0.6375	0.8516
	PC(O-18:0/2:0)	0.0459	0.0038	0.0749	0.0159	0.0457	0.0099	0.2598	0.0875	0.0091	0.0607	0.0170	0.0588	0.0118	0.4301	4.2180	0.4324
	PC(O-12:0/2:0)	0.0933	0.0240	0.0935	0.0203	0.0371	0.0095	0.1673	0.0560	0.0202	0.0615	0.0141	0.0391	0.0096	0.5974	1.1890	0.8516
	PC(O-18:3/2:0)	0.0746	0.0161	0.0878	0.0176	0.0801	0.0313	0.8963	0.0865	0.0236	0.0857	0.0230	0.0848	0.0257	0.9990	0.4165	0.8848
	PC(O-20:4/2:0)	0.1114	0.0093	0.1377	0.0091	0.1840	0.0731	0.4234	0.1211	0.0236	0.2044	0.0304	0.1723	0.0579	0.3392	0.3824	0.8848
	PC(O-20:4/2:0)	0.1631	0.0333	0.1785	0.0436	0.1837	0.0482	0.9533	0.1922	0.0380	0.2335	0.0369	0.2014	0.0581	0.7688	0.5759	0.8516
	PC(O-14:1/2:0)	0.2046	0.0717	0.1867	0.0428	0.1232	0.0359	0.6745	0.1160	0.0378	0.1968	0.0567	0.1500	0.0254	0.5387	1.0930	0.8516
	PC(O-18:1/2:0)	0.1570	0.0150	0.2087	0.0345	0.2072	0.0361	0.5278	0.1400	0.0385	0.3103	0.0922	0.2396	0.0699	0.3946	0.4114	0.8848
	PC(O-16:2/2:0)	0.1746	0.0491	0.1937	0.0359	0.1670	0.0519	0.8997	0.2032	0.0685	0.2077	0.0541	0.1617	0.0377	0.8375	0.3393	0.8848
	PC(O-16:0/2:0)	0.1812	0.0514	0.2517	0.0591	0.2801	0.1087	0.6797	0.2214	0.0074	0.2428	0.0527	0.3508	0.0639	0.2794	0.7741	0.8516
	PC(O-20:6/2:0)	1.8325	0.5205	2.0051	0.3198	1.5117	0.4624	0.7026	1.7615	0.5458	2.0371	0.4513	1.3571	0.2326	0.5915	0.0401	0.9574
	PC(O-14:0/2:0)	4.2494	0.9932	4.1089	0.7725	2.9											



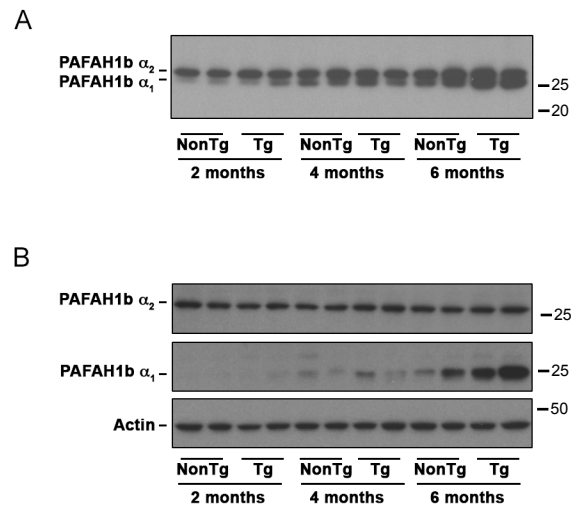
Supplemental Figure 1. Land's cycle metabolism of glycerophosphocholines. We use nano-ESI-LC-MS/MS to profile the repertoire of monoacylglycerophosphocholines (LPC), monoalkylglycerophosphocholines LPC(O), monoalkenylglycerophosphocholines LPC(P) (middle panel), 1-acyl,2-acetyl glycerophosphocholines (PC-PAF), 1-alkyl,2-acylglycerophosphocholines (PC(O)-PAF) and 1-alkenyl,2-acylglycerophosphocholines (PC(P)-PAF) (bottom panel). Lyso-glycerophosphocholines are generated by the hydrolysis of PC, PC(O), or PC(P) membrane precursors (top panel). Hydrolysis is mediated by a superfamily of phospholipase A₂ (PLA₂) enzymes, segregated into 16 groups and broadly distinguished by five discrete types. Lyso-glycerophosphocholines can be further modified by LPCAT1-4 to either regenerate a structural membrane glycerophosphocholine using acyl-CoA as a substrate (top panel) or produce PAFs, using acetyl-CoA as a substrate (bottom panel). Canonical PAFs are defined by their alkyl-linkage at the sn-1 position and their acetyl group at the sn-2 position (PC(O)-PAF). PAF-like lipids can have an sn-1 acyl-group (PC-PAF) or alkenyl-group (PC(P)-PAF) and up to 2-6 carbons at the sn-2 position. These second messengers are themselves both the products and the immediate precursors of lyso-glycerophosphocholines in the Land's cycle as they are remodelled back to their respective lyso-metabolites by PAFAHs. Abbreviations: cPLA₂, cytoplasmic phospholipase A₂; iPLA₂, calcium-independent phospholipase A₂; LPLA₂, lysosomal phospholipase A₂; LPCAT1-4, lysophosphatidylcholine acetyltransferase 1-4; PAF, platelet activating factor; PAFAH, platelet activating factor acetylhydrolase; PLA/AT, the H-RAS-like suppressor enzymes with both PLA₁ and PLA₂ activities as well as O-acyltransferase activities; sPLA₂, secretory phospholipase A₂.



Supplemental Figure 2. Verification that sphingomyelins are not detected in our glycerophosphocholine metabolite and second messenger LC-ESI-MS/MS profiles. Because sphingomyelins or lyso-sphingomyelins also fragment with a diagnostic m/z 184.1 ion, prior to molecular identification, we verified that all metabolites/second messengers profiled in this study were glycerophosphocholines using differential mobility spectroscopy. All details are as in Materials and Methods. No sphingomyelins or lyso-sphingomyelins were detected in our targeted m/z range of 450-650.



Supplemental Figure 3. Analysis of critical glycerophospholipidome metabolites in 4-month old hypoxic compared to normoxic WT mice. Neither normoxic aging or exposure to hypoxia significantly altered the cortical WT lipidome. Univariate analysis revealed that no species were significantly altered in WT mice challenged with hypoxia or by age. Data represent mean log₂ fold change of 6-9-month normoxic WT and 4-month hypoxic WT compared to 4-month normoxic animals. Statistics were one-way ANOVAs. (All ANOVAs: $p > 0.05$).



Supplemental Figure 4. Western analysis of PAFAH α_2 and α_1 catalytic subunits. (A) Higher exposure of immunoblot presented in Fig. 5 demonstrating that the α_1 subunit is detected at low levels in younger mice with protein expression increasing with age. As indicated in Fig 4, blots were probed simultaneously for α_1 and α_2 . (B) To confirm these results, the same proteins were run in a replicate immunoblot and probed sequentially for α_2 (top panel), stripped and reprobed for α_1 (middle panel), and stripped and reprobed for the actin loading control (bottom panel). PAFAH α_1 protein levels increased in both NonTg and Tg mice with age. Levels appeared to increase more robustly in older Tg animals compared to NonTg but these genotypic differences were not statistically significant (see densitometry in Fig. 5).